

1

Gecko-Inspired Nanomaterials

Christian Greiner

1.1

The Gecko and Its Adhesion Capabilities

Scientific interest in the gecko began when, more than 2000 years ago, the Greek philosopher Aristotle first coined the phrase “..like the Gecko lizard” [1]. Since then, this lizard’s amazing ability to climb walls and run on ceilings has inspired a wealth of research studies, many of which have proposed reasons for the gecko’s amazing adhesive abilities. However, it was not until the 1960s that the German anatomist Uwe Hiller made a major breakthrough when, using electron microscopy, he revealed the bristle-like, hierarchical structure of the gecko’s toe pads [2, 3] that today, are recognized as being responsible for the animal’s climbing abilities. The next key player to provide an understanding of the nature of those fibrillar adhesives was Keller Autumn who, by using a microelectro-mechanical system (MEMS)-type apparatus was able to measure the adhesive properties of one gecko seta (a hair on the toe pad; see below), and subsequently revealed that the gecko’s adhesive abilities relied mainly on van der Waals forces [4].

1.1.1

What are Setae?

On examining more closely the hierarchical nature of the gecko adhesive system (Figure 1.1), the structure is based on the *lamellae*, from which the individual adhesive hairs—the *setae*—protrude. The setae, which are about 20 μm in diameter and 130 μm long [4], split into many smaller and finer hairs; this resembles the structure of the branches of trees, where a one large trunk ends up in very small twigs. Following this analogy, the leaves at the end of the branches are termed *spatulae*, due to their similarity in appearance to a spatula. The tiny spatula, which are about 200 nm long, 200 nm wide, and about 20 nm thick [4], make contact with the substrate on which the gecko is walking. However, as the van der Waals forces are about as weak as they are omnipresent, the gecko must rely on having between

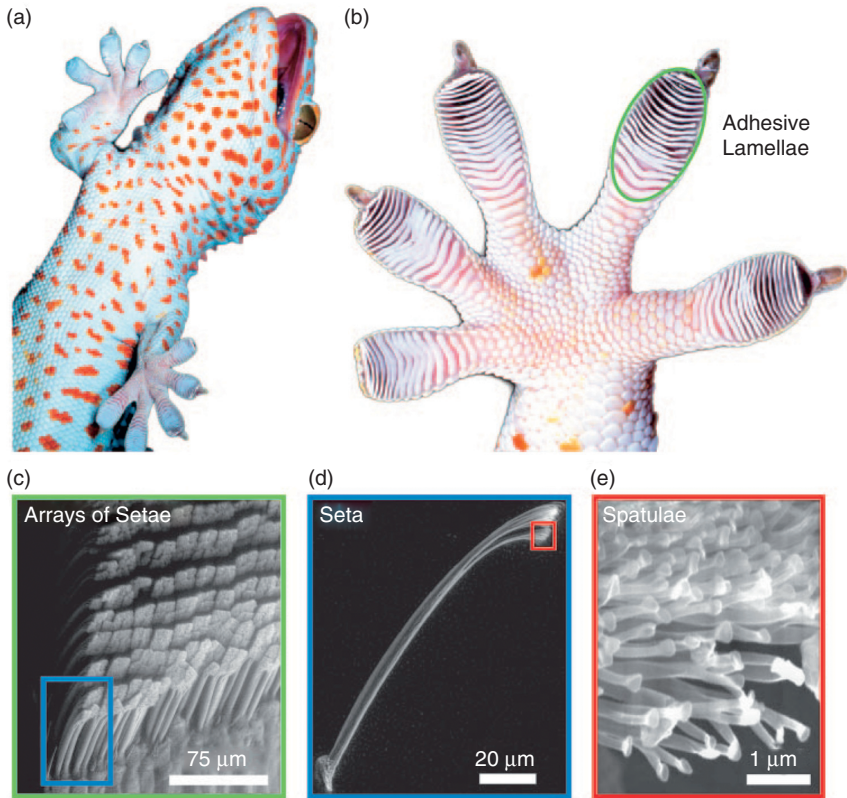


Figure 1.1 Illustration of the hierarchical nature of the gecko adhesive system. (a) Macrostructure: A tokay gecko climbing on glass; (b) Mesostructure: View of the foot, with the adhesive lamellae (highlighted by the green oval) on one toe; (c) Microstructure: An array of setae made

visible in a SEM image; (d, e) Nanostructure: SEM images of a single seta with its branched structure, terminating in hundreds of spatular tips. Reproduced with permission from Ref. [8]; © 2005, National Academy of Sciences, USA.

50 and 500 million spatulae on each toe pad [4]. Hence, subsequent atomic force microscopy (AFM) measurements of individual setae revealed that the gecko has a safety factor of not less than 10 [5,6]. An additional important finding of this was that capillary forces do play a role in gecko adhesion, and that adhesion is increased in line with humidity [6].

It should be noted that the gecko is not the only animal possessing such a fibrillar adhesive system; indeed, many insects and arthropoda exhibit the same type of structure (see Figure 1.2), including beetles, flies and spiders [7]. However, the gecko—as the heaviest of these animals—possesses the most hierarchical adhesive systems, and thus the most amazing adhesion capabilities.

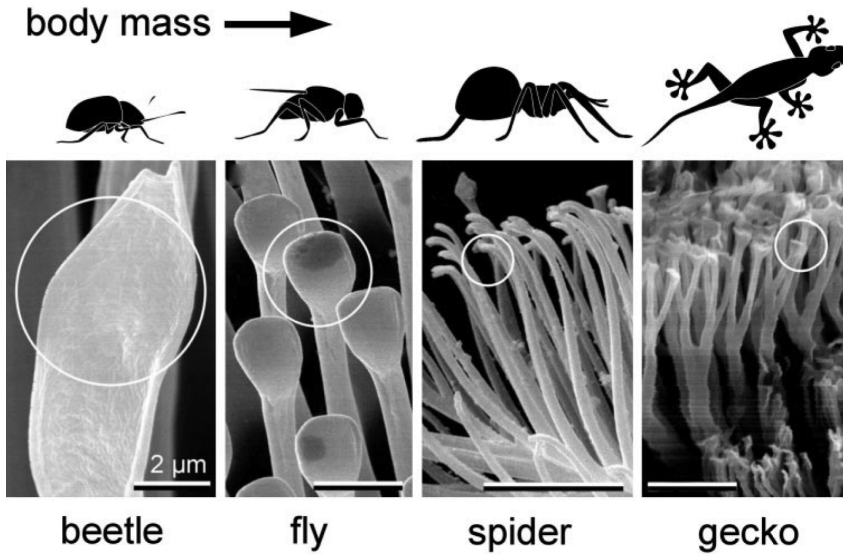


Figure 1.2 Terminal elements (circles) in animals with hairy design of attachment pads. Note that the heavier animals exhibit finer adhesion structures. Scale bar = 2 μm .

Reproduced with permission from Ref. [7]; © 2003, National Academy of Sciences, USA.

1.1.2

Walking on the Ceiling

In discussing the gecko's amazing adhesive qualities, whilst an ability to walk on vertical structures and ceilings is remarkable, the gecko also has a fully reversible, self-cleaning adhesive system. Whilst man-made adhesives are either strong (e.g., Super-glue) or reversible (e.g., sticky pads), the gecko system has both properties—it is strong and fully reversible, and does not leave behind any residue (as would Scotch tape). Moreover, whilst a sticky pad would not adhere to dust, and subsequently would not stick elsewhere due to dust accumulation on the adhesive region, the gecko can run through an environment such as fine sand and yet, after a couple of steps on a clean surface, the adhesive structure has become clean! In an attempt to reveal the basis of this self-cleaning process, Kellar Autumn used silica-alumina microspheres to clog the gecko's toe pads, and then measured the adhesive force of the foot [8]. Then, in a similar study using clean gecko feet, Hansen and Autumn showed the gecko's toe pads to have recovered about 50% of their initial (clean) adhesion performance after only four steps [8]. This high safety factor of the gecko system is easily sufficient for the animal to maintain a reliable adherence. To explain this self-cleaning behavior, Hansen and Autumn proposed a system whereby a silica–alumina particle (representing a dust particle)

would be in contact with the substrate on one side, but with only a limited number of spatula on the other side. It was calculated that, depending on the size of the dirt particles (in this case, a radius of ca. $2.5\ \mu\text{m}$), the adhesive force on the substrate would be greater than that on the spatulae. In other words, the gecko could “shake-off” the dust particles one by one (or better, step by step) until the adhesion performance was sufficiently strong to support the animal’s body weight, and this occurred after only about three steps [8].

The question remains, therefore, as to why these adhesive abilities of geckos and other animals with fibrillar adhesive systems might be important in the life sciences. Clearly, the abilities of these animals has inspired the widespread development of man-made fibrillar adhesives, with two recent reviews having been produced by Chan *et al.* [9] and del Campo *et al.* [10]. Whilst the first review focuses on the physical principles of adhesion and on the parameter space available (see below), the second relates to the different fabrication methods available. Recently, attempts have been made to render fibrillar adhesives available to the life sciences, ranging from drug delivery systems [11] to gecko-inspired bandages [12]. A review of the physical principles behind gecko adhesion will be provide in the following subsections, together with discussions of the design space and the first applications in the life sciences.

1.2 The Physics of Gecko Adhesion

1.2.1 Contact Splitting

The main principle behind gecko adhesion, termed *contact splitting*, was first suggested by Arzt *et al.* [7, 13]. Although, at first glance it might seem counter-intuitive that the removal of material from a contact region can enhance adhesion, both theoretical and experimental evidence has accumulated showing that patterning—that is, the splitting of one solid contact into many finer contacts—is indeed beneficial. This general principle might be better understood by considering the following examples.

First, when peeling one material from another at an interface (Figure 1.3a), the applied force (P_s) is proportional to the width (w_s) of the interface by the interfacial adhesion (G_c) [14]: $P_s = G_c \times w_s$. For this reason, the peeling of a wider piece of tape will require more force than for a thinner tape. When peeling all regions of a representative patterned area simultaneously, for a close-packed configuration of n regions (Figure 1.3b), the increase in interfacial width scales as $n^{1/2}$. Thus, the total peel force P_n also increases as $n^{1/2}$ for a patterned interface as compared to a nonpatterned interface. The dependence on the so-called *contact line* rather than the contact area, for controlling adhesion was demonstrated by several groups studying patterned adhesives [15–17]. This simple relationship demonstrated that the maximum separation force could be increased, whereas the total energy of

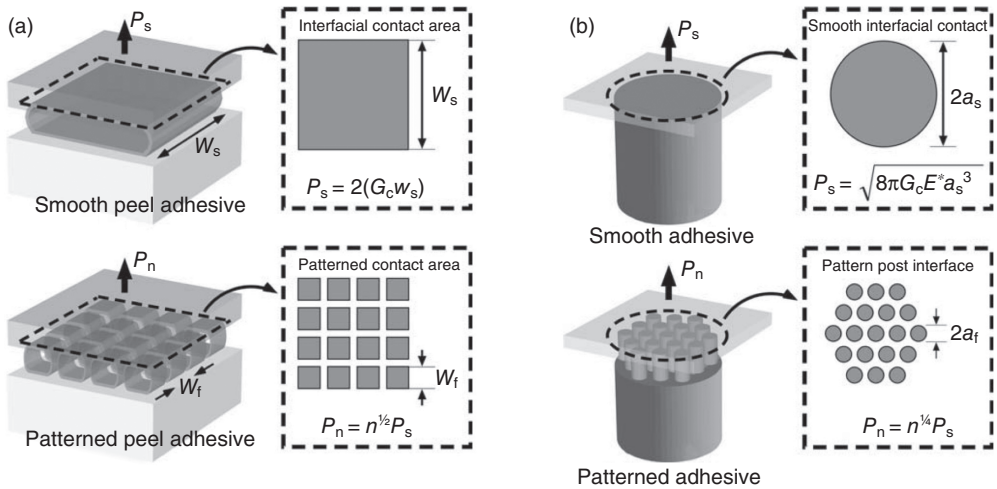


Figure 1.3 Examples demonstrating the principle of contact splitting. For both examples, the separation force of the patterned adhesive (P_n) increases with the total number of split-up contacts (n), which illustrates that the enhancement in strength is associated with the increase in contact line, as opposed to contact area. (a) In a peel

geometry, $P_n \sim n^{1/2}$; (b) In a flat-punch geometry, $P_n \sim n^{1/4}$. G_c is the interfacial adhesion, a_s is the smooth contact radius, E^* is the reduced Young's modulus, and P_s is the separation force for a smooth reference. Figure reproduced from Ref. [9]; © 2007, Materials Research Society.

separation would actually decrease because of a reduction in the interfacial contact area. In order for patterns to increase both total force and total energy, the energy associated with initiating separation at the perimeter of an individual post must be greater than the energy of propagation away from the perimeter. This may be caused by differences in mechanical constraints, and has been demonstrated to cause significant increases in adhesion for some patterned interfaces [15, 18–20].

A second example of how patterns may change the interfacial contribution can be explained by considering the perpendicular separation of a pillar from a flat surface (e.g., a finger pulling away from a sticky surface) (Figure 1.3b). In this case, it can easily be shown that the force to separate n posts (P_n) scales directly with the separation force of a single post (P_s) [21]: $P_n = n^{1/4} P_s$. The scaling changes if the posts are terminated with spherical caps of a curvature R . In this situation, Johnson–Kendall–Roberts (JKR) theory [22] predicts that $P_n = n^{1/2} P_s$ [7], such that the interfacial strength is enhanced by reducing the diameter of the pillars [23]. Similar to the peeling examples above, the energy of separation is enhanced only if the initiation energy is greater than the propagation energy.

Although the example mechanisms discussed here consider energy dissipation only at the interface, the three-dimensional (3-D) geometry of a patterned interface also has an important role to play. In this case, the aspect ratio of the features

increases the structures' compliance to the contacting surface; features with a higher aspect ratio conform more easily, and this improves their adaptability to rough surfaces. Increasing the aspect ratio of the features also effectively “blunts” any interfacial cracking during separation.

In addition to G_c , n , and λ , numerous additional parameters can influence the development and measurement of the adhesion for a patterned interface. One limitation for high-aspect ratio features is the tendency for nearest-neighbors to stick together because of interfeature attractive forces. The ultimate fracture force of the fibrils also decreases as the fiber diameter decreases, thereby limiting the smallest practical feature size. Spolenak *et al.* [24] were the first to propose a theory relating the balance of these design parameters in adhesion maps for patterned surfaces, and this concept will be described in more detail in the following subsection.

1.2.2

Adhesion Design Maps

As noted above, the parameter space for the design of artificial fibrillar adhesives is vast as it includes, among others, the fiber radius, Young's modulus, the aspect ratio, the tip shape, and the packing density. Due to this complexity, many different approaches for the fabrication of bioinspired fibrillar adhesives have been reported, as will be illustrated here. In order to help guide the materials selection process, the concept of adhesion design maps was proposed by Spolenak *et al.* [24] for a hemispherical contact geometry. A typical design map, as developed by these authors, is shown in Figure 1.4, where the radius of the fiber is plotted on the ordinate and the Young's modulus on the abscissa (these two elements are considered the most important design parameters). The fiber radius is of particular importance, as the above-mentioned “principle of contact splitting” demands for small fibers to increase adhesion. That this principle has its limits in real design problems and cannot be carried on *ad infinitum* is nicely illustrated in the maps, which visualize design guidelines and limiting factors:

- The *limit of fiber fracture* comes into play as fibers become increasingly thinner. In fact, at one point they are so thin that their internal strength, when modeled by the theoretical fracture limit, is less than the adhesive strength between the fiber tip and the counter surface. As a consequence, the fiber would rather break than loosen its adhesive contact; this would in turn constrain the reusability of the fibrillar systems and clearly must be avoided.
- The *limit of fiber condensation* (or matting, clumping, crowding) is an even more stringent factor, whereby when very thin and long fibers are packed too densely they tend to stick to each other rather than to the counter surface. This effect—termed *condensation*—leads to a dramatic reduction in adhesive strength [16].
- The *limit of ideal contact strength* acknowledges that there is an upper, theoretical limit for the adhesive strength of the van der Waals forces.

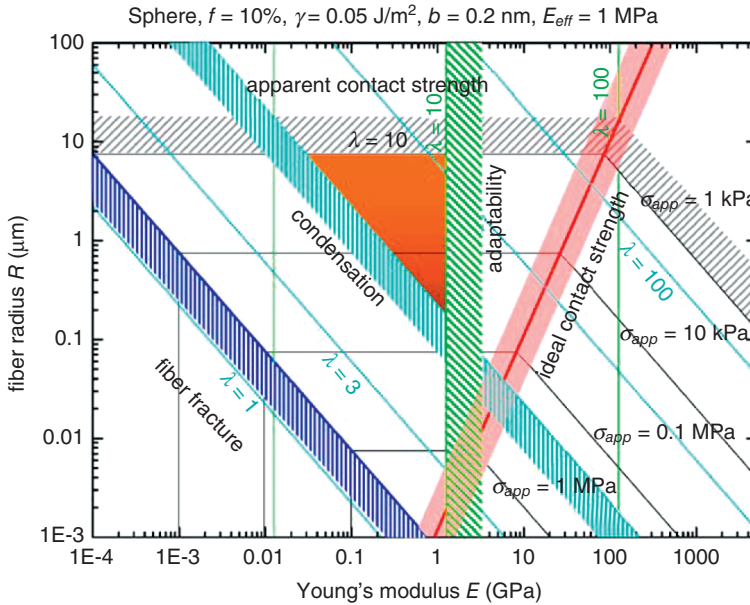


Figure 1.4 Typical adhesion design map for spherical contact elements, as developed by Spolenak *et al.* The blue line indicates the criterion of fiber fracture, the red line the ideal contact strength. The limit of fiber condensation is indicated by the cyan lines, and adaptability by green lines. The black lines are contours of equal apparent contact strength. Reproduced with permission from Ref. [24].

- The *limit of adaptability* takes into account that a certain compliance of the entire fibrillar structure is necessary in order to ensure adhesion also to rough surfaces.
- The *limit of apparent contact strength* was introduced by Spolenak *et al.* in order to set a lower limit for the adhesive strength; this must be met by the structures if they are to be useful adhesives at all.

As mentioned previously, the parameter space for fibrillar adhesive is vast, while the adhesion design maps in their current form represent only a first, albeit very instructive, means of systematizing the different constraints in the design process. Future developments will have to acknowledge the influence of different tip shapes on adhesion (see Section 1.5.3), and for the roughness that real surface always have. Some effort has already been made in this direction, as reported by Greiner *et al.* [25], who provided examples of adhesion design maps for pillars that showed a flat punch and a toroidal contact geometry. In addition, when the case of fibers with the geometry of an elastic tape were examined, this proved to be much closer to the natural “role model” and could be clearly demonstrated by calculating the optimal adhesive angle for the tape structures (this turned out to be very similar

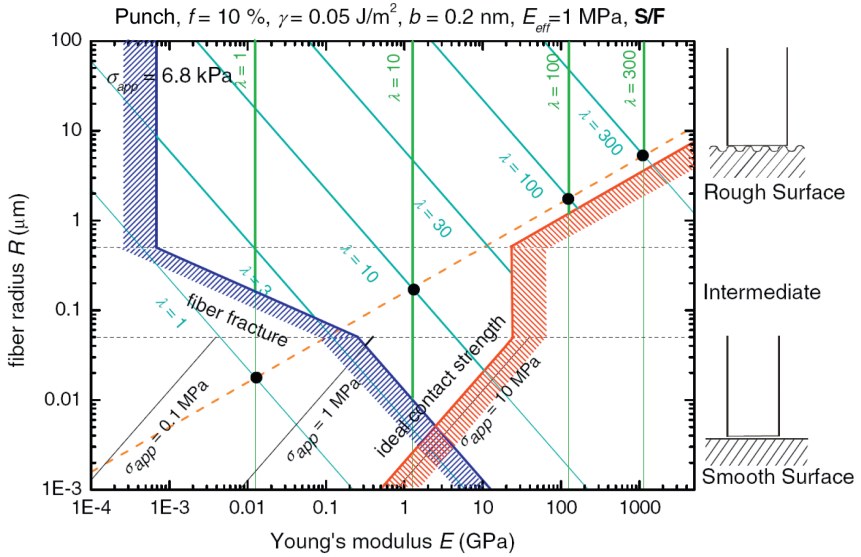


Figure 1.5 Adhesion design map for a flat tip against a substrate with periodical roughness. For the surface roughness, a radius of the small spheres of $a = 500 \text{ nm}$ is considered. The dashed, orange line is the “conode.” For $R > 500 \text{ nm}$, the presented model for flat tips against a rough surface is employed. For

$R < a$, the apparent contact strength is constant over the entire map—contact splitting invariance—and the minimum Young’s modulus is determined by the fiber fracture limit. Reproduced with permission from Ref. [26].

to that of the gecko fibrillar system, at ca. 55°). An example of a design map that takes into account surface roughness is shown in Figure 1.5. Whilst this might be only a first step, it clearly shows that adhesion design maps represent a versatile tool for visualizing the design parameters that are important for fibrillar adhesives, and might also prove very useful in the future development of such systems. Finally, it must be stressed that, despite the many simplifications made (some of which were quite severe) when constructing the maps, these predictions have proven to be intriguingly accurate.

1.3

Fabrication Methods for Gecko-Inspired Adhesives

1.3.1

Soft-Molding

Among the most common methods used to fabricate fibrillar adhesives, the best-known is that of *soft lithography* [27]. The term itself is applied to a collection of pattern-replication methods which rely on an elastomeric mold [27, 28]. The latter

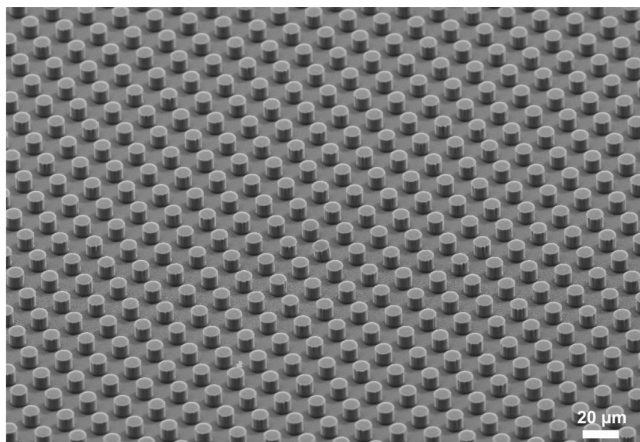


Figure 1.6 SEM image of a PDMS test surface structured via soft lithography. The pillars are $10\mu\text{m}$ in radius and have an aspect ratio of 1. The image demonstrates the high quality and homogeneity of soft-lithographic structures.

is a negative replica of a microstructured or nanostructured hard master, and is prepared by casting and thermally curing a liquid prepolymer (most often poly(dimethylsiloxane); PDMS) on the master. The PDMS replica can be considered as the final patterned surface (Figure 1.6), or it can also be used as a mold (or stamp) for patterning other polymeric materials in subsequent replication processes. The elastomeric character of the PDMS stamp allows it to be released easily from the master (or molded polymer), even in the presence of complex and fragile structures, such as high-aspect ratio fibers. Moreover, its low interfacial free energy and chemical inertness reduce the degree of mold sticking.

One prerequisite for soft-molding is access to masters with a desired geometry. The masters for bioinspired fibrillar adhesives consist of arrays of holes with predefined dimensions, and have been typically fabricated by photolithography [15, 16, 29, 30]. Alternatively, masters have been produced by indenting a wax surface with an AFM tip [31], or by the laser ablation of a metallic surface [32]. Photolithography using an SU-8 photoresist has been proven particularly suited to obtaining regular model surfaces in which the influence of the different geometric parameters on adhesion can be characterized and quantified [16]. This resist material has been specially formulated to obtain high-aspect ratio features, such as holes, which are required to obtain long PDMS fibers in the replication process [33]. Arrays of fibers with radii of 1 to $25\mu\text{m}$ and lengths of 5 to $80\mu\text{m}$ have been reported over 25cm^2 areas [16]. These systems have been used to analyze the influence of contact radius and aspect ratio of the fibers in the final adhesion performance of the artificial adhesive surface [16]. In theory, soft-molding allows the fabrication of fibers of any dimensions, but in reality the aspect ratio of the fibers is limited by the low mechanical stability of the PDMS, with fiber collapse

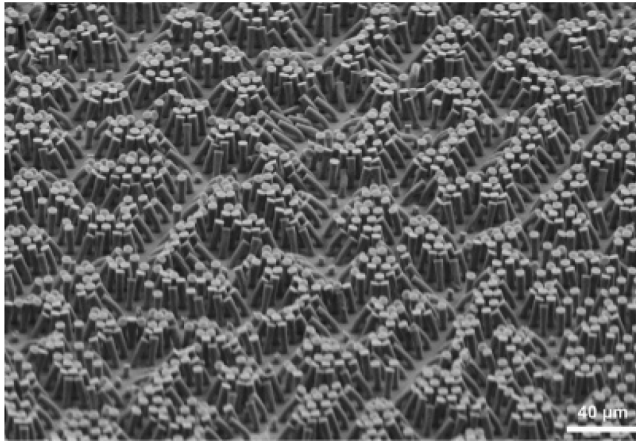


Figure 1.7 SEM image showing an array of pillars made by soft-molding Sylgard 184 onto SU-8 photolithographic templates. The pillars have a radius of $2.5\ \mu\text{m}$ and a height of about $20\ \mu\text{m}$. The image highlights the collapse of pillars with hexagonal symmetry. Reprinted with permission from Ref. [16].

typically occurring in micron-sized fibers with aspect ratios in excess of 4 (Figure 1.7). This fact is more critical in nanosized fibers, the fabrication of which requires the use of harder materials.

Soft PDMS stamps can be also applied to generate fibrillar micropatterns of different materials by soft-molding polymer melts, polymer solutions, or polymer precursors. For example, PDMS stamps have been used to soft-mold liquid polyurethane precursors, such that fibers with $20\ \mu\text{m}$ diameter, 40 to $100\ \mu\text{m}$ length and $40\ \mu\text{m}$ spacings were obtained [34]. In addition, PDMS is transparent and can be used to mold UV-curable prepolymers; in this case, hard polyurethane patterns with fibrils of 0.5 to $4\ \mu\text{m}$ height and diameters ranging from 1 to $4\ \mu\text{m}$ have been created [30].

Tilted fibrillar structures are required if reversible gecko-inspired adhesives are to be fabricated. The tilted disposition of the fibers allows the adhesive to be peeled-off, and therefore easily removed [35]. Tilted SU-8 fibrils have been obtained via photolithography by tilting the mask and the resist film with respect to the beam during exposure, using a tilting stage. In this way, soft-molding polyurethane precursors with a PDMS negative replica of the SU-8 master yielded arrays of polyurethane microfibers with a tilting angle of 25° [34]. By using a polyurethane instead of PDMS, the group of Metin Sitti from Carnegie Mellon University also created several fibrillar adhesives with tilted pillars [34, 36]. In another very interesting approach, Pokroy *et al.* [37] fabricated nanoposts with different tilt angles via a two-step soft-molding process where, in the second step, the PDMS mold was stretched, compressed, and torsioned in various ways.

1.3.2

Nanostructured Adhesive Surfaces

1.3.2.1 Hot Embossing

Thermoplastic materials can be patterned by the process of *hot embossing*, in which a polymer melt is shaped by the conformal contact of a microstructured or nanostructured mold, using heat and pressure. The polymer melt is able to flow and fill the mold cavities under the processing conditions. The filling depends on the viscosity of the melt, its wetting properties and pattern geometry, as well as on applied pressure or vacuum. Solidification of the polymer after filling is achieved by cooling below the crystallization temperature in semicrystalline polymers, or below the glass transition temperature (T_g) in amorphous polymers. Removal of the mold releases a structured polymer with features that reproduce its particular geometry; this is achieved by either peeling-off (demolding) or by a selective dissolution of the template. Demolding is preferred as it permits the same mold to be used for additional molding processes. The embossing process was carried out at temperatures above the T_g of poly(methylmethacrylate) (PMMA) ($\sim 120^\circ\text{C}$), using a polyurethane acrylate mold, such that arrays of fibers of 150 nm diameter and up to 500 nm in height were obtained [38, 39]. The fabrication of high-quality molds represents one of the most important requirements for successful embossing. These molds are typically prepared from silicon or silicon dioxide by dry-etching technologies, or by the deposition of nickel or other metals on patterned resist substrates, via the LIGA (Lithographie, Galvanofomung, and Abformung-process) process. Since mold fabrication is the most time- and cost-consuming step of these patterning techniques, it is likely to constitute the greatest limitation in potential industrial applications.

1.3.2.2 Filling Nanoporous Membranes

Track-etched polycarbonate (PC) and anodic alumina (AA) membranes have been used as low-cost alternatives to expensive molds for producing arrays of long, nanosized fibers [31, 40, 41]. These membranes are commercially available, with pore sizes ranging from a few nanometers to a few micrometers, and with different spacings and thicknesses. The pores of the membrane can be filled with polymer precursors, solutions or melts so as to obtain a structured polymer film possessing cylinders with dimensions that reproduce those of the pores (Figure 1.8). This method has been used quite extensively for the first examples of fibrillar adhesives [31, 40, 41].

PC membranes containing randomly distributed cylindrical pores of $0.6\ \mu\text{m}$ diameter and spacings $<5\ \mu\text{m}$ have been filled with poly(imide) (PI) solutions [40]. As the PC membrane is flexible, it can be peeled-off from the solidified PI film to release dense arrays of high-aspect ratio nanofibers. Due to their large aspect ratio, these fibers were shown to collapse laterally, and therefore a reduced adhesion would be expected. AA membranes with pores of 200–400 nm diameter have been also filled with a two-parts epoxy resin [40], with a polystyrene (PS)

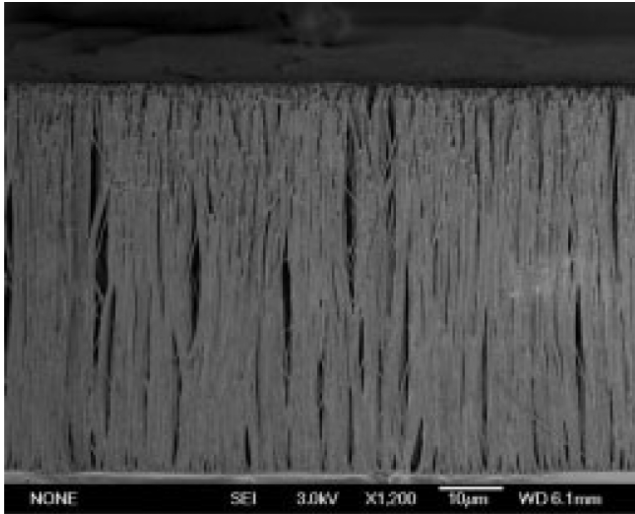


Figure 1.8 Cross-sectional view of as-prepared and vertically aligned polystyrene nanotubes fabricated through the filling of a porous membrane. Note the bundling of the fibers. Reproduced with permission from Ref. [41]; © Wiley-VCH Verlag GmbH & Co. KGaA.

solution [41], and with UV-curable precursors [42]. Because of their rigidity, AA membranes cannot be removed from the polymer by peeling-off, but rather need to be dissolved selectively in NaOH solution. Unfortunately, this represents a major disadvantage for fabrication, as the template is destroyed, while dissolution takes a long time and may also cause polymer swelling. Wet etching is also followed by a drying step, during which capillary forces usually may cause lateral collapse and, consequently, reduced adhesion (Figure 1.8) [42]. Similar problems of fiber condensation were also reported by Kim *et al.* [43], who used colloidal nanolithography to fabricate the mold for their parylene nanopillars.

1.3.2.3 Electron-Beam Lithography

Arrays of PI fibers have been microfabricated using electron-beam lithography (EBL), followed by pattern transfer via dry etching in an oxygen plasma [44]. The etching step is necessary in order to obtain high-aspect ratio structures, as the maximum penetration depth of low-energy electrons is only about 100 nm. The diameters of the fibers produced ranged from 0.2 to 4 µm, the heights from 0.15 to 2 µm, and the spacings from 0.4 to 4.5 µm. Whilst this method is appropriate for obtaining model nanostructures with smaller dimensions than are obtained via optical photolithography, the patterning is slow, is restricted to small areas, and also requires an electron-beam facility to be available.

1.3.2.4 Carbon Nanotubes

Microfabrication techniques strongly restrict the material's selection to some resists, all of which are quite expensive. In addition, patterning can only be carried out in specialized laboratories (clean rooms), and requires costly equipment and long processing times. For this reason, the quest has begun for alternative patterning techniques that do not require a template (e.g., the mold in soft-lithography or the mask in photolithography). Consequently, arrays of vertically aligned carbon nanotubes (CNTs) have been reported as an interesting alternative [45–50]. CNTs have smaller diameters (10–20 nm) than gecko spatulae (~200 nm), and may also be made with high length (>65 μm [46]). In having an extremely high aspect ratio, exceptional mechanical strength, and excellent electronic and thermal properties, CNTs show great potential for dry adhesion applications with additional electrical/thermal management capabilities (e.g., electroswitching, through-thickness thermal transport, high-temperature use) [45]. Arrays of CNTs have also been fabricated via chemical vapor deposition (CVD) on Si substrates, where the nanotubes were aligned almost perpendicular to the substrate surface and had a fairly uniform tubular length. Unfortunately, however, they tended to stick to their closest neighbors, forming loosely-packed “bundles” that reduced the overall adhesive force of the CNT layer due to a lesser number of contact points. Arrays of CNTs were successfully transferred from the Si wafer to flexible backing substrates [46, 47]. For this purpose, the patterned silicon wafer was embedded in a polymer precursor and, after curing, the CNTs were peeled-off from the wafer. By etching the silicon-facing side of the polymer matrix, either by solvents or through plasma treatment, a smooth layer of CNTs was generated on a flexible backing.

1.3.2.5 Drawing Polymer Fibers

Arrays of nanofibers have been obtained by drawing fibers from polymer drops on nonwetttable surfaces by contacting them with a hot plate and then moving the two surfaces apart [51]. This process is based on surface tension and capillary forces, and is available in several versions. For example, films of thermoplastic polymers can be brought in contact with a hot structured master possessing pillars; subsequently, when the master and the polymer are pulled apart, fibers will be drawn from the contacting points. Alternatively, structured polymer films with large features can be brought in contact with a hot surface and then removed, so as to obtain elongated fibers on the top of the features [51]. Others have developed a miniaturized version of this method by using an AFM tip to draw nanosized fibers from a melt polymer film [52]. Although these fabrication methods seemed more suited to large-area patterning, and were therefore more likely to be applied in manufacturing systems, the production of nanosized fibers would require a concise alignment between the hot plate (or roll) and the polymer film, across large areas.

An ingenious alternative was reported recently which avoided alignment problems by combining the molding and fiber drawing processes so as to obtain high-aspect ratio nanofibers from thin PS and PMMA films [53]. This was achieved by carrying out the demolding step at temperatures above the T_g -values

of the materials. Capillary forces induced a deformation of the polymer melt into the void spaces of the mold, and the filled nanofibers were elongated upon removal of the mold due to a tailored adhesive force at the mold/polymer interface.

1.3.2.6 Hierarchical Adhesive Surfaces

A hierarchical organization of fibers over different length scales (nm to mm) mimics the multiple levels of compliance present in gecko setae, which is required for adaptability and adhesion to rough surfaces of any form.

1.3.2.6.1 Multistep Exposure in Photolithography Lithographic fabrication by superposition of the coating and irradiation steps enables the fabrication of structures with several organization levels, using traditional two-dimensional (2-D) set-ups and alignment markers on the mask to guide the superposition. The fabrication procedure is shown schematically, together with an example of an adhesive structure with two hierarchical levels obtained by SU-8 in Figure 1.9 [33, 54]. Additional levels are possible simply by increasing the number of coating and irradiation steps. The geometries are not restricted to cylindrical fibers, and depend only on the mask used for the irradiation. This process can be replicated using soft-molding methods, and transferred to other materials [54].

1.3.2.6.2 Microfabrication Technologies Hierarchical structured surfaces have also been obtained by combining photolithography and dry-etching methods, as typically used in MEMS fabrication [55–57]. In this case, single-crystal silicon posts (1 μm in diameter, and up to 50 μm high) supporting microsized silicon dioxide platforms (2 μm thick, 100–150 μm wide) were coated by photoresist fibers with ~ 250 nm diameter and ~ 4 μm height on average. In another approach, Murphy *et al.* [58] fabricated hierarchical microfibrillar adhesives by first fabricating angled polyurethane fibers (as described in Section 1.3.1), followed by a dip-transfer process to form flat mushroom-shaped tips in the micron range (the adhesion properties of these structures will be discussed later).

1.3.2.6.3 Filling Stacked Membranes Hierarchical patterns were obtained by filling stacked microporous and nanoporous AA membranes with different pore diameters [59]. The nanoporous membrane (pore diameter ~ 60 nm, interpore distance ~ 100 nm) was generated by the anodization of an aluminum film in an oxalic acid solution. The microporous alumina was produced by conventional lithography and anisotropic chemical etching of a thick film of anodic alumina pores. The microporous and nanoporous alumina membranes were subsequently brought into intimate contact and filled with a PMMA solution. Hierarchical polymeric microfibrils (fibril diameter ~ 10 μm ; fibril length ~ 70 μm) with nanofibril arrays at their tips were obtained following removal of the solvent by heating, and after selective etching of the AA membranes [59]. The nanofibrils had a lateral dimension of approximately 60 nm, and aspect ratios as high as 100:1.

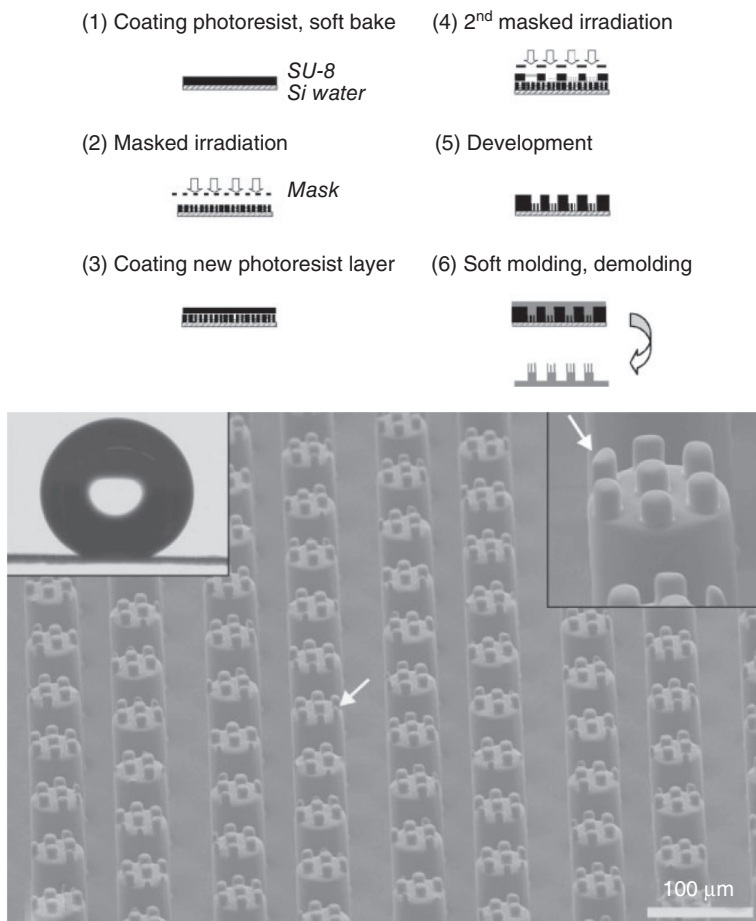


Figure 1.9 Schematic of the processing steps for the fabrication of hierarchical PDMS pillars through two-step photolithography and soft-molding. The lower panel shows an SEM image showing an array of hierarchical pillars fabricated by soft-molding Sylgard 184 on SU-8 photolithographic templates. The base-pillars have a radius of $25\ \mu\text{m}$ and a height of $200\ \mu\text{m}$. The top pillars have a

radius of $5\ \mu\text{m}$ and an aspect ratio of 1. The right-hand insert shows a close-up of the hierarchical structure; the left-hand insert shows a water droplet resting on the structure (contact angle 160°). The arrows indicate pillar sections. Reproduced with permission from Ref. [54]; © Wiley-VCH Verlag GmbH & Co. KGaA.

1.3.2.6.4 Two-Step Embossing By performing two sequential embossing steps, hierarchical patterns with micrometric fibers decorated with nanosized fibers of various sizes and spacings were obtained [38]. A PMMA film was patterned with microfibers using a PDMS stamp; subsequently, nanofibers were patterned on top of the preformed microfibers, using a hard polyurethane acrylate (PUA) mold. The

PUA mold replaces the PDMS mold for sub-100 nm lithography, since high-aspect ratio sub-100 nm features in a PDMS mold do not retain dimensional stability, due to the low Young's modulus of PDMS. The resultant micro/nanoscale combined structures were robust, and demonstrated enhanced water-repellent properties as a consequence of the hierarchical arrangement.

1.3.2.7 3-D Structured Adhesive Surfaces

The 3-D geometry of the tip seems to be crucial for the adhesion performance of a fibrillar surface, with spherical, conical, filament-like, band-like, sucker-like, spatula-like, flat and toroidal tip shapes having been observed in different animals [60]. The role of the contact geometry has also been analyzed in artificial model systems [17], with a study conducted by del Campo *et al.* revealing that the contact shape had a strong influence on adhesion [17]. Using a modification of the soft-molding method, arrays of PDMS fibers with spherical and spatula-like tips have been reported [17, 61, 62]. The fabrication methods employed are shown in Figure 1.10. Here, arrays of pillars with spherical and spatular tips were obtained by inking PDMS fibrillar surfaces in a thin film of the PDMS precursor. A small drop of precursor remained on the top of the pillars. Curing of the array in an upside-down orientation yielded hemispherical tips as a consequence of gravity and surface tension acting on the fluid drop. Alternatively, the inked stamp could be pressed against a flat substrate and then cured, so as to create pillars with a flexible

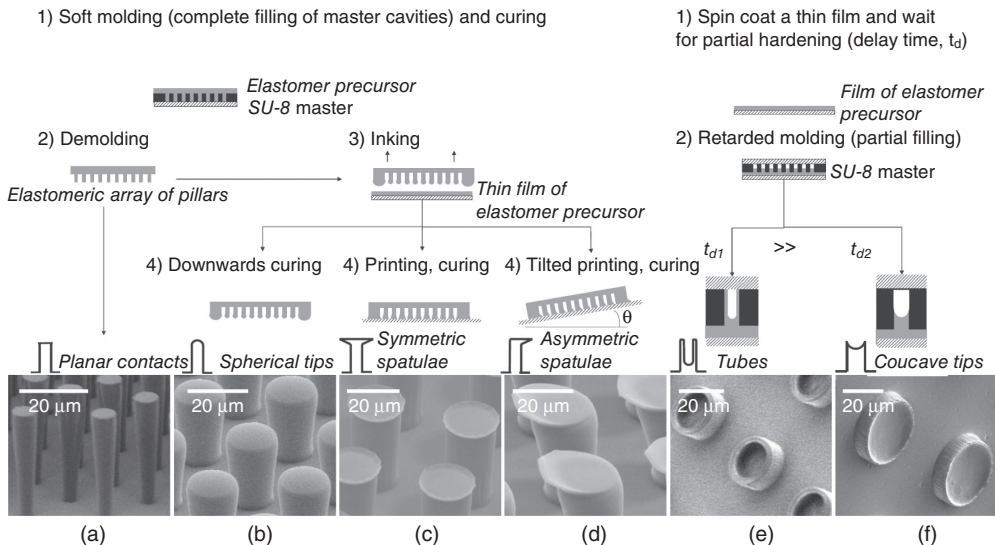


Figure 1.10 Overview of the fabrication strategies for PDMS pillars with different tip shapes, as developed by del Campo *et al.* The SEM images (a–f) show examples of the structures obtained. Reproduced with permission from Ref. [61];

© Wiley-VCH Verlag GmbH & Co. KGaA.

and flat roof and with a diameter that depended on the thickness of the spin-coated film. The roofs may be either symmetric or asymmetric, depending on the tilt of the substrate during curing. Others have used this method to obtain a continuous thin film of PDMS on top of a fibrillar surface, which also seems to be advantageous for adhesion purposes [63]. A similar approach was taken by Murphy *et al.* for their hierarchical structures [58]. Spatula-like fibers have been fabricated by filling prefabricated 3-D masters that had a negative profile with Teflon, followed by removal of the master by etching [64].

1.3.2.8 Switchable Adhesive Surfaces Made from Responsive Materials

Patterning technologies can be combined with responsive polymer materials to create microstructured surfaces with a switchable adherence. The application of an external field (e.g., magnetic) causes changes in the topographic design, and this influences the final adhesion performance. When a shape-memory polymer was selected for this purpose, arrays of microfibers with diameters between 0.5 and 50 μm and heights between 10 and 100 μm were patterned by soft-molding (Figure 1.11) [66]. Mechanical deformation of this topography at the shape-memory transition temperature, followed by cooling to room temperature in the deformed position, yielded a temporary nonadhesive surface that consisted of pillars in a tilted position. By reheating above the transition temperature, however the patterned surface switched from the temporary nonadhesive state to a permanent adhesive surface, with an at least 200-fold increase in adhesion.

Northen *et al.* [57] chose another approach for the fabrication of a switchable adhesive (images of their structures are shown in Figure 1.12). In this case, after having fabricated the paddles, a thin nickel layer was deposited before they were coated with an organic layer. Plasma-treatment of the organic layer led to the formation of “nano hairs.” Since nickel is ferromagnetic, the paddles turned by 90° in a magnetic field, thus reducing the adhesion properties to completely non-sticky. The advantage of this method over the approach described above was that the shape-memory polymer could be switched only once, whereas the nickel paddles could be moved more or less endlessly. Other approaches to switchable adhesives were taken by Lin *et al.* [67], who made use of the wrinkles in adhesives by stretching a PDMS-based structure, whilst Xie and Xiao [68] used a shape-memory polymer to create a self-peeling adhesive.

1.4 Measuring Adhesion

1.4.1 What Actually is Measured?

For elastic materials with a smooth interface, adhesion is often described by the critical adhesion energy, G_c . This descriptor represents the critical driving force for moving a “crack” at the interface, and has units of energy per area. If the

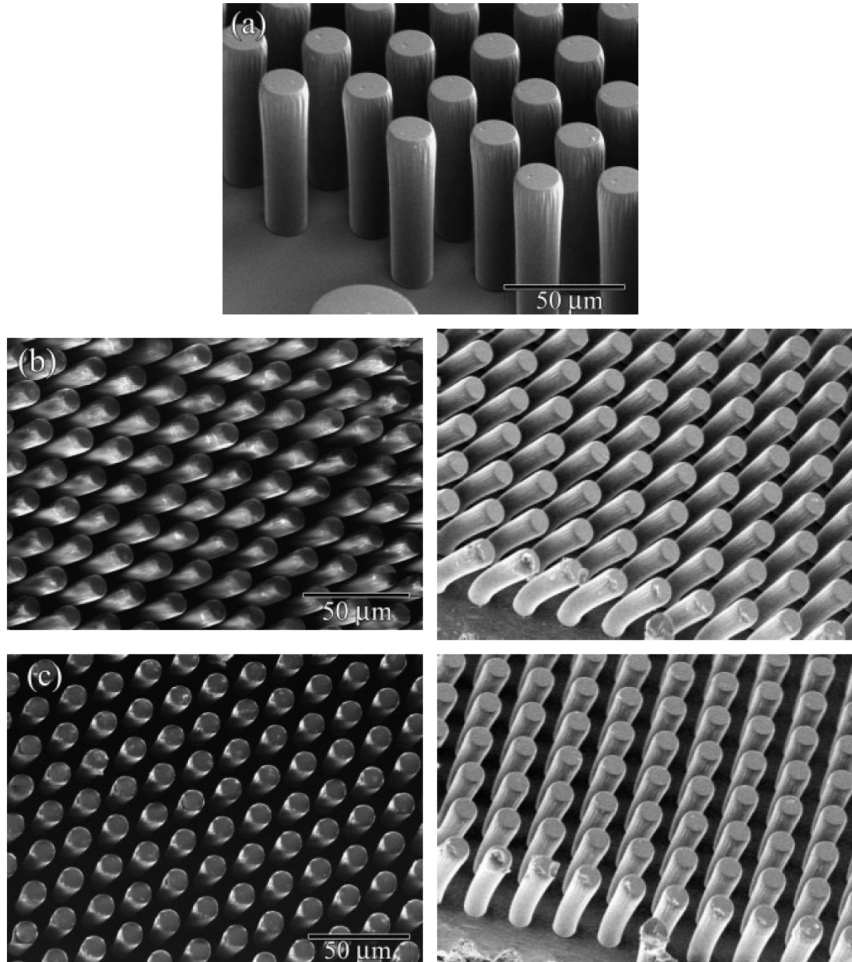


Figure 1.11 SEM images of Tecoflex pillars with $r = 10\mu\text{m}$, $h = 100\mu\text{m}$ and $20\mu\text{m}$ interpillar spacing. (a) Original pattern; (b) Top (left) and side (right) views of tilted pillars after deformation at 70°C and fixation

in the deformed state by cooling below T_{trans} ; (c) Top (left) and side (right) views of recovered pillars after reheating at 70°C . Reproduced with permission from Ref. [65]; © Wiley-VCH Verlag GmbH & Co. KGaA.

applied driving force is greater than a critical value (G_c), then the two materials will separate. When G_c is known for a given pair of materials, the practical design parameters such as the maximum sustainable force or stress for a given geometry can be determined. Frequently, contact probe adhesion tests are used for both patterned and nonpatterned interfaces.

In *contact probe testing*, a probe is brought into contact with another material, and the established interface is subsequently separated [18, 69, 70]. During the entire test, the force (P), the displacement (δ), and the contact area ($A = \pi a^2$, where a is the radius) are monitored and provide a complete description of the adhesion

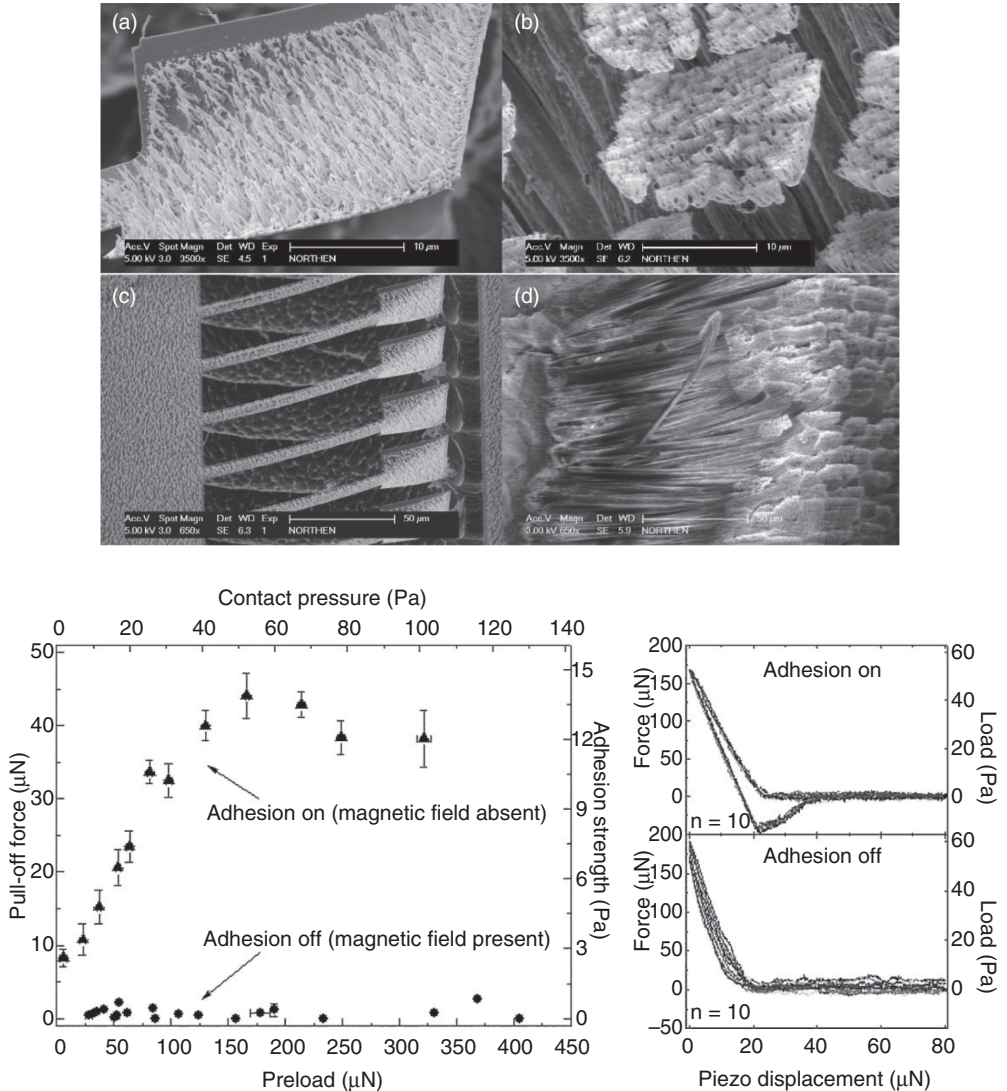


Figure 1.12 (a–d) Electron microscopy images of synthetic structures (left) and the analogous gecko structures (right), samples from a Tokay gecko (*Gekko gekko*). (a) Paddle surface coated with evenly spaced uncondensed aligned vertical polymer nanorods; (b) The branched terminus of a seta into spatula (same magnification, scale bar = 10 μm); (c) Freestanding nickel cantilevers and paddles coated with nanorods; (d) An array of setae (same magnification, scale bar = 50 μm). The lower panels show adhesion results, demonstrating the on/off behavior of the structures without and with an

applied magnetic field, respectively. The insets represent actual adhesion data, where in the “ON” state distinctive pull-off events were observed (top), and in the “OFF” state no pull-off events were observed (bottom). In the “ON” state, the devices showed an initial increase in adhesion with preload force, characteristic of increased surface contact with applied load (this was most likely a result of slight misalignment between the 5 mm flat punch and the test surface). Reproduced with permission from Ref. [57]; © Wiley-VCH Verlag GmbH & Co. KGaA.

properties. These measured parameters can be used to calculate G_c using existing theories, and from this the maximum separation force and stress can be determined. The direct relationship between G_c and these adhesion descriptors depends on the probe geometry. For a spherical cap, JKR theory was used to derive the following equation: $P_c = 1.5\pi G_c R$, where R is the radius of curvature [22]. For a circular punch of radius a , $P_c = k^* (a^3 G_c)^{0.5}$ was found by Maugis and Barquins [21]. Here, k is a constant related to the elastic properties of the materials at the interface. Based on these relationships, for a spherical cap, P_c is independent of the elastic properties as well as the maximum contact area. For a circular punch, P_c is dictated by both the elastic properties and the dimensions of the interface. Normalizing P_c for a circular punch by the interfacial area to define an average stress (σ_c), shows that σ_c is still dependent upon dimensions and materials properties: $\sigma_c = k_1^* (G_c/a)^{0.5}$.

For patterned interfaces such as those described in this chapter, G_c cannot be defined quantitatively, and consequently most research groups use descriptors such as P_c , σ_c , and a term called W_{adh} ; the latter is defined as the energy dissipated during contact and separation normalized by the maximum contact area [15]. It is very important to note that whilst these quantities are useful, they do not represent absolute properties. W_{adh} , for example, will not approach thermodynamic quantities for fully reversible materials, and is dependent on the maximum contact area. Additionally, P_c will depend upon the contact history, such as the maximum contact force and the number of contacting cycles [71]. In practice, all of the measurement techniques discussed below rely on measuring a force–distance curve, as shown in Figure 1.13. The pull-off force P_c is determined as the difference between the part of curve where the two surfaces are not in contact and the minimum of the curve; here, pull-off occurs. It should be mentioned at this point that, in “real” experiments—and especially in those with patterned surfaces—pull-off does not occur suddenly but sometimes a lot slower and over a considerable distance (see Figure 1.13). This behavior can be explained by the thermodynamics of the process (but this would be beyond the scope of the chapter).

1.4.2

How is Adhesion Measured?

As with fabrication methods, and also in the way that the adhesive strength and performance of adhesive systems are evaluated, a wide variety of testing methods has been developed. Some of these are rather crude; an example is the method of Geim *et al.* [44], in which the macroscopic adhesive properties of a material were measured using a laboratory balance. A similar approach was taken by Qu and Dai [45] and by Zhao *et al.* [48], who also tested their CNT-based adhesives by using a laboratory balance to quantify the adhesion forces.

Most of the other approaches were much more refined, however, with some relying on AFM. For example, Yurdumakan *et al.* [46] performed adhesion measurements on their adhesive by using a standard scanning AFM probe tip. AFM-based testing methods were also used by others, such as Sitti and Fearing [31],

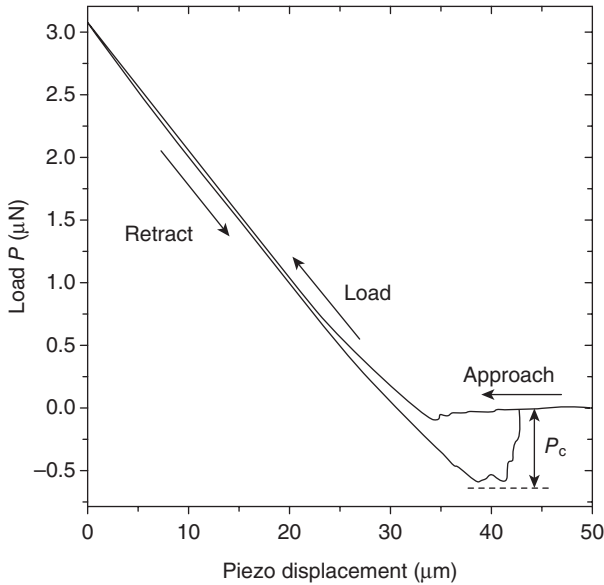


Figure 1.13 Real load–displacement curve obtained from a patterned surface with $r = 25\ \mu\text{m}$ and an aspect ratio of 1. A saw-tooth profile can be observed during retraction before pull-off occurs, as is often the case for structured surfaces. Reprinted with permission from Ref. [16].

who measured the adhesion properties of individual bumps with a tipless AFM cantilever. In addition to the balance measurements mentioned above, Geim *et al.* [44] tested the adhesive properties via AFM with a custom-made flat cantilever. Kim *et al.* [42], glued glass microspheres of $20\ \mu\text{m}$ diameter to the end of an AFM cantilever, similar to Yoon *et al.* [39], who investigated the adhesion and friction properties of nanopatterned PMMA surfaces by gluing a borosilicate ball to a cantilever. AFM-based techniques were also applied by Kustandi *et al.* [72] and by Lu *et al.* [50].

Varenberg *et al.* developed a home-built adhesion testing set-up [73], which allowed for testing in vertical and lateral directions and for a flat-on-flat contact scheme through a self-aligning system; the contact area was visualized using high-magnification video microscopy. Jin *et al.* determined the adhesion force by means of a highly sensitive microelectromechanical balance system, which could measure the force needed to pull-off a water droplet from the nanofiber surface [41]. Crosby *et al.* [15] and Thomas and Crosby [18] used a home-built set-up which indented the test surfaces with a polished fused silica sphere (5 mm radius), whereby the contact area was monitored *in situ* using an inverted optical microscope. A similar approach was taken by Kim and Sitti, by Aksak *et al.* [34] and by Murphy *et al.* [74], as well as by Cheung and Sitti [75], to test fibrillar adhesives, but with a 6 mm glass sphere attached to a load cell, and also by Greiner *et al.* [16, 17, 61, 76], who used

a glass cantilever and a 5 mm sapphire ball. Glassmaker *et al.* [77] also used a home-built set-up which measured load and displacement, and also allowed the contact area to be observed via an optical microscope, to test poly(vinylbutyral) samples against glass slides and, later, against PDMS pillars [29, 78, 79] and film-terminated [63] fibrillar adhesives against a glass sphere. Kim *et al.* [80] used a silicon disk of 0.43 mm radius attached to a load cell and a motorized stage to quantify adhesion values, and investigated the effects of backing the layer thickness. Peressandko and Gorb [32] used a micromanipulator and a load cell; in this case, the contact area was monitored using video microscopy so as to evaluate the adhesion performance of a poly(vinylsiloxane) (PVS)-based adhesive. A similar apparatus without the microscope, but with the capability to measure shear forces, was developed by Yao *et al.* [81]. Again, a similar equipment for quantifying adhesion values was used by Verneuil *et al.* [82] to investigate the adhesion of microstructured elastomer surfaces, but in this case a rubber bead was used at the end of a cantilever, while the deflection was measured using a laser beam. Another approach to a custom-built adhesion tester was taken by Santos *et al.* [83], who used a three-axis positioning stage to move the samples and bring them in contact with substrates attached to a six-axis force and torque sensor to measure these quantities. In particular, these authors investigated the effect of the pull-off angle with this set-up. In addition to this variety of custom-built set-ups, a commercial Hysitron nanoindenter was used by Northen *et al.* [55, 56, 84], which used a spherical aluminum tip [55] and an aluminum flat punch [56] as indenters. In addition, Pfaff measured adhesion with a commercial MTS NanoXP nanoindentation system [85].

1.5

What Have We Learned About Fibrillar Adhesives?

1.5.1

Contact Splitting

One of the most interesting points when considering fibrillar adhesives is the principle of contact splitting. As discussed above, the division of one contact area into a number (n) of contact elements enhances adhesion by a factor of n^r , where the exponent r describes the efficiency of the contact splitting for a particular contact shape [60]. The mechanism of contact splitting was observed for synthetic fibrillar adhesives, as demonstrated by comparing the pull-off strength σ_c versus the fibril radius a_f for a variety of sizes and shapes (Figure 1.14) [16, 17].

As the data in Figure 1.14 indicate, smaller fiber radii lead to a higher pull-off strength, as predicted by theory. The tip geometry of the fibrils plays also an important role in the splitting efficiency of the pattern (this is discussed further below). The dimensions of the individual fibrillar features must also relate to the roughness dimensions of the contacting surface, in order to take advantage of the splitting effect. This was demonstrated with natural examples by Huber *et al.* [86], and with synthetic analogs by Crosby *et al.* [15]. When testing surfaces with pillars

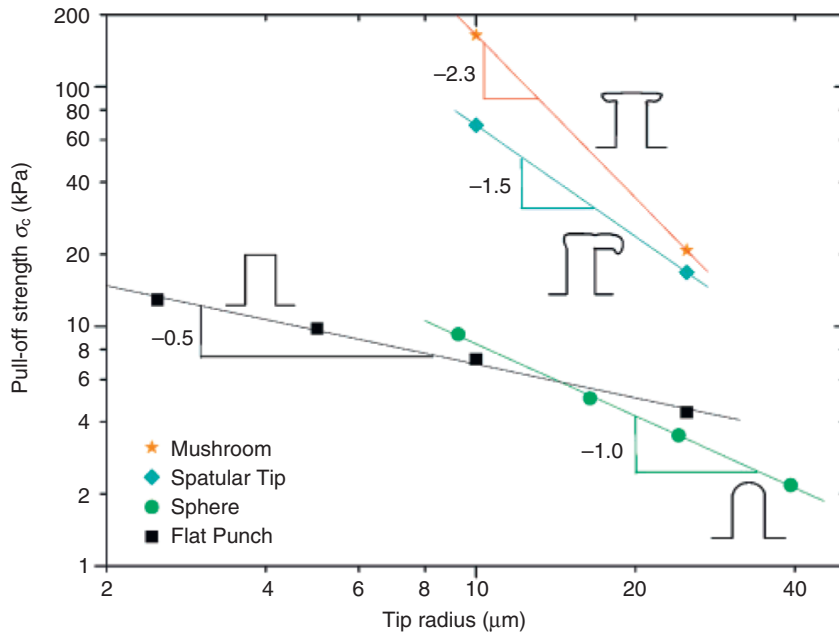


Figure 1.14 Tip radius dependence of the pull-off force (“splitting efficiency”) for flat, spherical, spatular, and mushroom-like contacts. The data correspond to a preload $P_p = 1$ mN. In the case of spherical tips, the radius corresponds to the radius of curvature measured by white light interferometry. For all other geometries, the pillar radius is used. Reprinted with permission from Ref. [17].

or with dimples (fabricated by punching flat PVS with a hollow needle) of different radii (20 to 120 μm), Varenberg *et al.* found that the pull-off force did not correlate systematically with the real contact area, but depended linearly on the real contact perimeter [19]. Although to date, this finding lacks theoretical explanation, it might be connected to the rather high surface roughness of these structures.

1.5.2

Aspect Ratio

The effect of aspect ratio is particularly interesting, as the experimental results obtained to date have been slightly contradictory. In one of the earliest studies, Zhao *et al.* [48] synthesized multiwalled carbon nanotubes (MWCNTs) with heights ranging between 5 and 10 μm , by CVD on silicon substrates. In order to measure adhesion, the samples were pressed against a laboratory balance with a preload of about 20 N, and then retracted. In repetitive experiments, Zhao *et al.* showed that the adhesion performance decreased over time, as some of the CNTs lost contact with the substrate. Interestingly, however, the pull-off force increased with

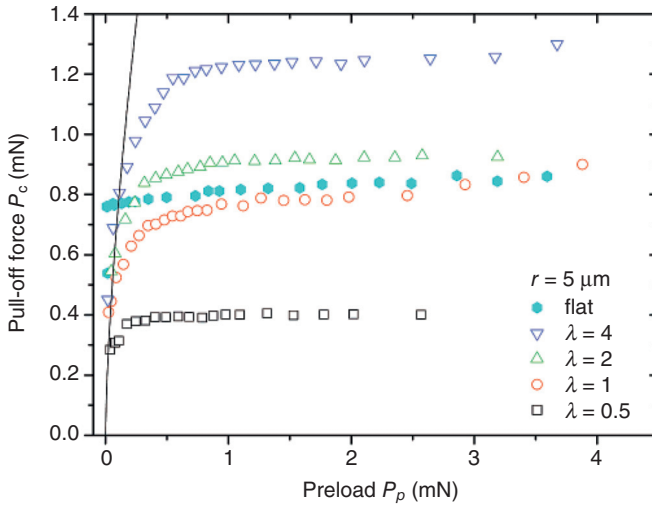


Figure 1.15 The influence of aspect ratio on the adhesion of patterned surfaces. The data correspond to pillar patterns with radius $5\ \mu\text{m}$ and different heights, measured at different preloads. The solid line corresponds to theoretical values according to the JKR theory. Reprinted with permission from Ref. [16].

decreasing fiber height, an effect which was neither understood nor explained by the authors, and went against all theoretical considerations. In general, the adhesion performance reported by these authors might have been artifactual, due to the very high preloads. No effect of the aspect ratio was found by Glassmaker *et al.*, who firmly bonded poly(vinyl butyral) (PVB) fibrils to glass substrates [77]. In contrast, Aksak *et al.* [34] identified an effect of the aspect ratio, whereby longer fibers adhered more strongly than shorter fibers. The same trend was also reported by Greiner *et al.* who, in a systematic study [16], showed the adhesion performance of fibrillar adhesives to increase with the fiber aspect ratio (see Figure 1.15). These results could be explained on the basis of a theory developed by Jagota and Benison [87], which was related to a previous model concerning the fracture behavior of rubbers [88] that had been developed during the 1960s. Basically, the higher the aspect ratio, the more elastic energy would be dissipated on pull-off, thus increasing the work of adhesion. Based on the results of this study and the agreement with theoretical predictions, the effect of a greater adhesion performance with an increase in fiber aspect ratio seems certain.

1.5.3

Tip Geometry

Among the four tip geometries shown in Figure 1.14, the mushroom-shaped tips clearly provided the most promising results [17, 61–64, 89, 90]. Similar to the fibrils

of the gecko, the mushroom design appears to “transfer” the applied energy away from the interface, with most of the energy being stored in the smaller, longer “stem,” which is significantly more geometrically compliant than the short, wide cap. Therefore, the energy gained by separating a small area of the cap would be insignificant, and the associated driving force for separation would be small. In addition to the effect on adhesion performance, Kim *et al.* [91] also showed that tip shape would influence the wet self-cleaning behavior of fibrillar adhesives. Specifically, they showed that mushroom-shaped fibers were significantly more hydrophobic than flat punch fibers, and thus would be more easily wet-cleaned. (It should be noted here that this is not yet the self-cleaning found with the gecko, but may be a step towards it!)

1.5.4

Young’s Modulus

To investigate the effect of Young’s modulus on fibrillar adhesives, Greiner *et al.* [25] created seven samples with different moduli by post-curing PDMS for increasing times. The moduli of these samples were obtained by fitting the compressive parts of the load–displacements curves (see Figure 1.13) to the Hertzian expression [92]:

$$p = \frac{4}{3} E^* \sqrt{R \delta^3} \quad (1.1)$$

where P is the applied compressive preload, R the radius of the indenting sphere, δ the indentation depth, and $E^* = E/(1 - \nu^2)$ the reduced Young’s modulus, with $\nu = 0.5$ as Poisson’s ratio. Reduced Young’s moduli between $E^* = 0.83$ and 1.23 MPa were obtained. According to the results measured, the pull-off force of the structured surfaces decreased with increasing PDMS stiffness (see Figure 1.16, which shows P_c and σ_c as a function of the effective Young’s modulus, E^*). A drop by a factor of 1.4 (from $P_c = 0.68$ mN to 0.49 mN) was measured when E^* was increased 1.5-fold ($E^* = 0.83$ MPa to 1.23 MPa). In Figure 1.16, it can be seen that the pull-off strength as a function of preload is constant for all samples, regardless of their E^* -value. The decrease in pull-off force with increasing modulus is apparently offset by a concomitant drop in contact area; thus, the pull-off strength, being the ratio between the two, remains constant.

1.5.5

Backing Layer

Until now, two groups have investigated the influence of backing layer thickness. In one such study, Greiner *et al.* [25] prepared PDMS samples with thicknesses of between 0.54 and 28.06 mm and showed that P_c fell weakly 1.1-fold ($P_c = 0.58$ mN to 0.64 mN at $P_p = 2.0$ mN) when the backing layer thickness was increased by a factor of more than 50. This was surprising, as it might have been expected that a thicker backing layer would promote not only an adaptation to surface roughness

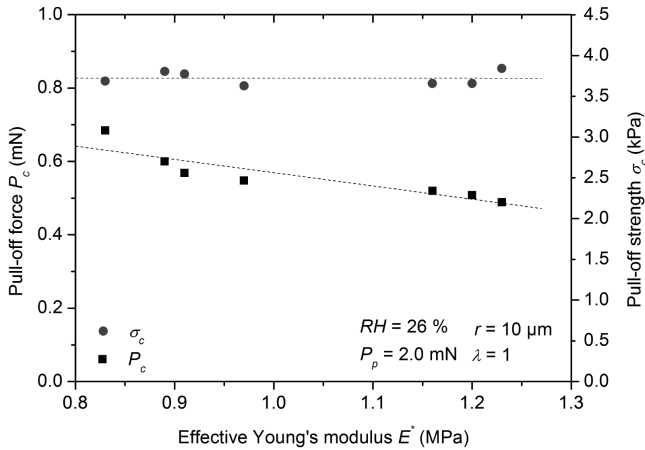


Figure 1.16 Effect of Young's modulus on adhesion (pillars of radius $r = 10\mu\text{m}$, aspect ratio $\lambda = 1$). The samples had different reduced Young's moduli, which were obtained through different curing conditions. Pull-off force and strength versus effective Young's modulus (at a preload of 2 mN). The broken lines were obtained through a linear fit to the data, which indicate the influence of modulus on the pull-off force and the lack of it in the strength. Reprinted with permission from Ref. [71].

but also an ability of the fibers to make contact due to an increase in effective compliance. However, this seemed not to be the case, and the pull-off strength showed less dependence on the backing layer thickness. Kim *et al.* [80] identified a similar effect when measuring mushroom-terminated polyurethane pillars with backing thicknesses ranging from 160 to 1120 μm against a flat silicon disk. For this sevenfold decrease in thickness, the pull-off force was increased by about a factor of 9; these differences were attributed to a more effective “equal load sharing” between the fibers with thin backing layers.

1.5.6

Tilt Angle

The effect of fiber tilt angle was investigated by Yao *et al.* [81] who, rather than fabricate free-standing PDMS pillars, created structures that were terminated by a closed PDMS film (similar to those prepared by Glassmaker *et al.* [63], Shen *et al.* [93], and Noderer *et al.* [94]). It was found that, for fiber tilt angles between 0° and 40° , the pull-off force would be increased by a factor of about 3. When Aksak *et al.* [34] also investigated the effect of tilt angle on the adhesion properties of fibrillar structures, they fabricated polyurethane fibers that were tilted about 25° from the vertical via a double-molding process from tilted SU-8 micropillars. Adhesion tests conducted on the tilted and untilted structures showed the adhesion performance to have been reduced by tilting, and this was attributed to a lower adhesion force per fiber in the tilted compared to the upright case. From the same group, Murphy *et al.* [74] tested angled fibrillar structures, but this time with

different contact shapes (spherical and mushroom). As these authors did not compare their data with that from upright pillars, no conclusions could be drawn regarding the effect of tilting on adhesion performance, although some interesting friction experiments were conducted. Santos *et al.* [83] investigated the effect of the pull-off angle for a special type of bioinspired fibrillar adhesive, and showed that both the pull-off force and work of adhesion were increased when the pull-off angle was decreased. Although surprising, these results proved to be valid since, for small angles, the experiments resembled a shear test rather than a pull-off experiment.

1.5.7

Hierarchy

Hierarchical arrays of fibrils have been fabricated by Kustandi *et al.* [72] by filling stacked alumina membranes that had different pore sizes. In this case, fibrils of 10 μm diameter and 70 μm length were decorated with nanofibers of 60 nm diameter and aspect ratios of up to 100. However, fiber collapse and clumping, which would cancel any beneficial effect that the hierarchical structure might have imparted [24], may have prevented adhesion measurements from being made. In a different approach, Northen *et al.* [55] microfabricated SiO_2 platforms on a flat silicon wafer, and coated them with irregular fibrils of ~ 200 nm diameter and ~ 4 μm length. The adhesion strength was shown to be $\sigma_c = 0.028$ kPa for the hierarchical structure, which was about four- to fivefold higher than for a fibril-coated flat silicon wafer without the platforms. In addition to these approaches, Greiner *et al.* [54] fabricated and tested hierarchical PDMS pillars. For this, the base pillars had a diameter of 50 μm and a height of 200 μm (aspect ratio $\lambda = 4$), while the top pillars had a diameter of 5 μm and heights ranging from 2.5 to 10 μm ($\lambda = 0.5$ –2). Other radii for the top pillars were also fabricated successfully. The pillars were found to be nonplanar on the top, but to have a finite curvature. The adhesion force as a function of compressive preload for the two- and single-level pillars are shown in Figure 1.17, from which it is immediately apparent that the two-level pillars adhered about 10-fold less than did the single-level structures with rounded edges (note the different scales on the ordinates); the same was true for the pull-off strength. This result was surprising, as theoretical studies had predicted a beneficial effect of hierarchy on adhesion [95–100], although an explanation was proposed that the effect was due to the low packing density of fibers and the rounded tip shape. Interestingly, a very recent study conducted by Murphy *et al.* [58] supported this theoretically predicted increase in adhesion, and confirmed that the energy dissipated during the pull-off process and the effective work of adhesion would be much larger for hierarchal adhesives than for single-level or even unstructured adhesives. Whilst this explains the gain in adhesion performance, it fails to explain why such a gain was not seen in the structures fabricated by Greiner *et al.*

It is most likely, however, that the gain was due to the rounded tip shape, since Murphy *et al.* had used mushroom-terminated fibers which, as noted in discussions regarding the effects of tip shape, are highly beneficial for adhesion behavior.

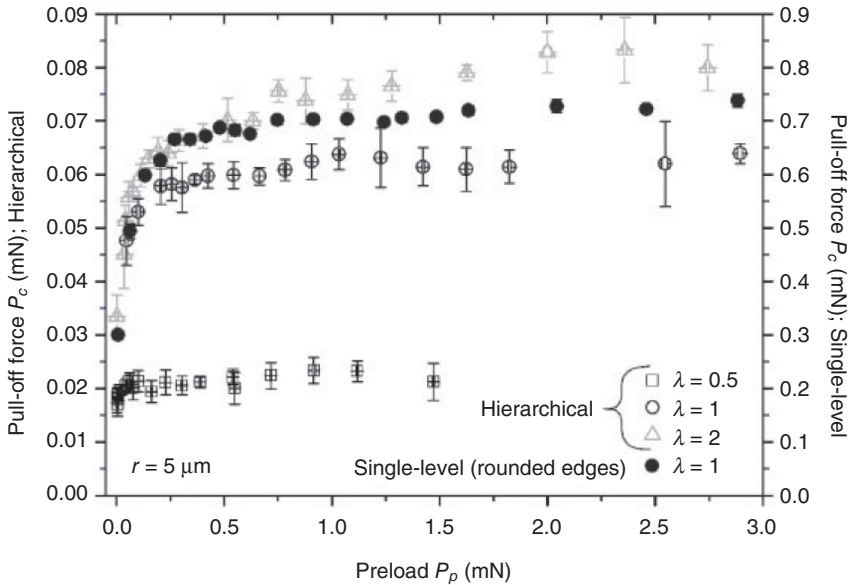


Figure 1.17 Effect of top-pillar aspect ratio on adhesion, plotted as pull-off force versus preload. The bottom pillars had a radius of $25\ \mu\text{m}$ and an aspect ratio of 4 in all experiments. The results for single-level pillars with the shape of punches with rounded edges and an aspect ratio of 1 have been added (scale on right ordinate). Reproduced with permission from Ref. [54]; © Wiley-VCH Verlag GmbH & Co. KGaA.

1.5.8

Experimental Parameters that Influence Measurements

1.5.8.1 Adhesion Tests: Indentation versus Peeling

Gorb *et al.* found that, for a flat-on-flat scheme used to quantify adhesion, the pull-off force did not depend on the preload [89]. The same authors also conducted peel tests and showed that, after cleaning a contaminated sample, a large part of the adhesion performance was recovered [89]. More recently, when Varenberg and Gorb studied the influence of shear on the pull-off behavior of the same pillars [101], they found that the pull-off force could be switched on and off, in a close to binary fashion, simply by moving the test stage through a certain lateral displacement (ca. $0.3\ \text{mm}$).

Interesting peeling experiments with biometrically patterned elastomer films were conducted by Ghatak *et al.* [102], who showed that small incisions in the films would increase the interfacial fracture toughness. By conducting very similar experiments, Majmunder *et al.* [103] investigated the effect of microchannels in flat elastomer substrates on crack trapping during peel testing, and demonstrated a remarkable (up to 30-fold) increase in adhesion performance. A somewhat

similar effect was reported by Glassmaker *et al.* [63] in peel tests with film-terminated fibrillar adhesives, where a ninefold enhancement in adhesion energy was found compared to a flat control. Lamblet *et al.* [30] also carried out peeling experiments on microstructured, fibrillar PDMS surfaces. When these authors investigated the influence of pillar aspect ratio and substrate rigidity, for low-aspect ratio pillars the soft substrates were more efficient, whereas for high-aspect ratio structures a stiff substrate tended to enhance adhesion. The peel testing of a CNT-based gecko-inspired adhesive was carried out by Ge *et al.* [47], who reported an extraordinarily high shear resistance for the structure, surpassing even the performance of the gecko almost fourfold. For the same adhesive, Sethi *et al.* [104] demonstrated self-cleaning lotus effect-like properties. A similar effect of self-cleaning in shear experiments was recently reported by Lee and Fearing [105], while Chan *et al.* [20] conducted 90° peel tests to investigate the influence of patterned reactive interfaces on the adhesion properties of fibrillar structures. Another approach for investigating fibrillar adhesives was taken by Schubert *et al.* [106], who used a “load–drag–pull” testing scheme, whereby a spherical indenter was attached to a two-axis force sensor. The indenter was brought into contact with the sample and dragged over its surface for a given displacement; the test probe was then retracted while measuring the adhesion forces. The applied shear force was shown to have a clear influence on the pull-off force. In the absence of any shear forces, the fibers showed very little adhesion, yet when the spherical indenter was being dragged a significant frictional adhesion was measured, and the adhesion was improved with use. Similar results were obtained in macroscopic tests carried out by Lee *et al.* [107], with the same types of sample. These representative reports show clearly that the performance of any given adhesive will depend heavily on the testing scheme used, and that the results of peel tests will most certainly differ from those of pull-off experiments. Clearly, it is important to select the test that is most comparable with the application in mind. It should be noted that, in many cases, this testing should include frictional components since, in reality, most adhesives will be loaded not only in tension but also in shear.

1.5.8.2 Indenter Geometry

When indenting with a sphere, the adhesion descriptors tend to depend on the indentation preload, an effect first identified Kim and Sitti [64] and by Greiner *et al.* [16]. Spherical indenters were used not only by these groups, but also by Crosby *et al.* [15] and Thomas and Crosby [18]. Flat-on-flat contact schemes are common among AFM-based techniques, such as those used by Sitti and Fearing [31]. This type of scheme—which included a system for self-alignment between the two surfaces—was developed by Varenberg and Gorb [73], who used the procedure extensively [19, 89, 101] to characterize a mushroom-shaped fibrillar adhesive system.

1.5.8.3 Humidity

Lu *et al.* [50] found no significant changes in adhesion values when investigating the adhesion and friction behavior of CNTs and fluoro-diamond films at relative

humidities between 5% and 60%. The same result was found by Greiner *et al.* [25] for a PDMS-based fibrillar adhesive, for humidities ranging from 2% to 90%. In a more detailed study using similar fibrillar adhesives, but also taking into account the effect of different contact sizes and shapes, Buhl *et al.* [108] demonstrated a more complex behavior, the details of which are beyond the scope of this chapter. In this case, the performance of fibrillar adhesives appeared to be decreased as the humidity increased, with the effect becoming stronger as the fibers became smaller. It was proposed, therefore, that a raised humidity might offset contact splitting.

1.5.9

Other Approaches and Factors

An interesting approach to improve the performance of fibrillar adhesives was taken by Lee *et al.* [109], who combined the adhesion principles found with geckos and mussels to create a so-called “geckel adhesive.” In these studies, when PDMS pillars were coated with DOPA (3,4-dihydroxy-L-phenylalanine), a protein used by mussels to cling to rocks, the required pull-off force was significantly higher than that of a fibrillar structure without DOPA. This effect was especially pronounced in the case of underwater adhesion, a scenario not yet considered. Varenberg and Gorb [110] also reported an increased adhesion of mushroom-shaped fibrillar adhesives if used underwater. Both of these findings suggested possible roles for new, glue-free underwater adhesives in environments ranging from marine to biomedicine. A recent attempt to increase the adhesion performance of fibrillar systems [75] involved the introduction of a silicon oil between the PDMS posts and a substrate. Whilst this no longer yielded a dry adhesive system that left no residues, many interesting applications were perceived.

1.6

Applications in the Life Sciences

In addition to oil-covered and underwater adhesives, which might have interesting applications in areas of biomedicine and the life sciences, several reports have been made proposing the similar use of fibrillar systems. For example, Mahdavi *et al.* [111] have described a biodegradable and biocompatible gecko-inspired fibrillar adhesive for biomedical applications that could be used either as a wound sealant or as a replacement (or augmentation) of surgical sutures and staples. For this, a biodegradable polymer [poly(glycerol-co-sebacate acrylate)] and a prestructured silicon template were used to generate the fibrillar structures (see Figure 1.18). In order to optimize the adhesive, different fiber shapes, lengths and spacings were tested in a liquid environment, and also with porcine intestinal tissue to mimic applications within the human body. A strong adhesive effect was demonstrated, as would be required for surgical sutures, and the structures proved to be

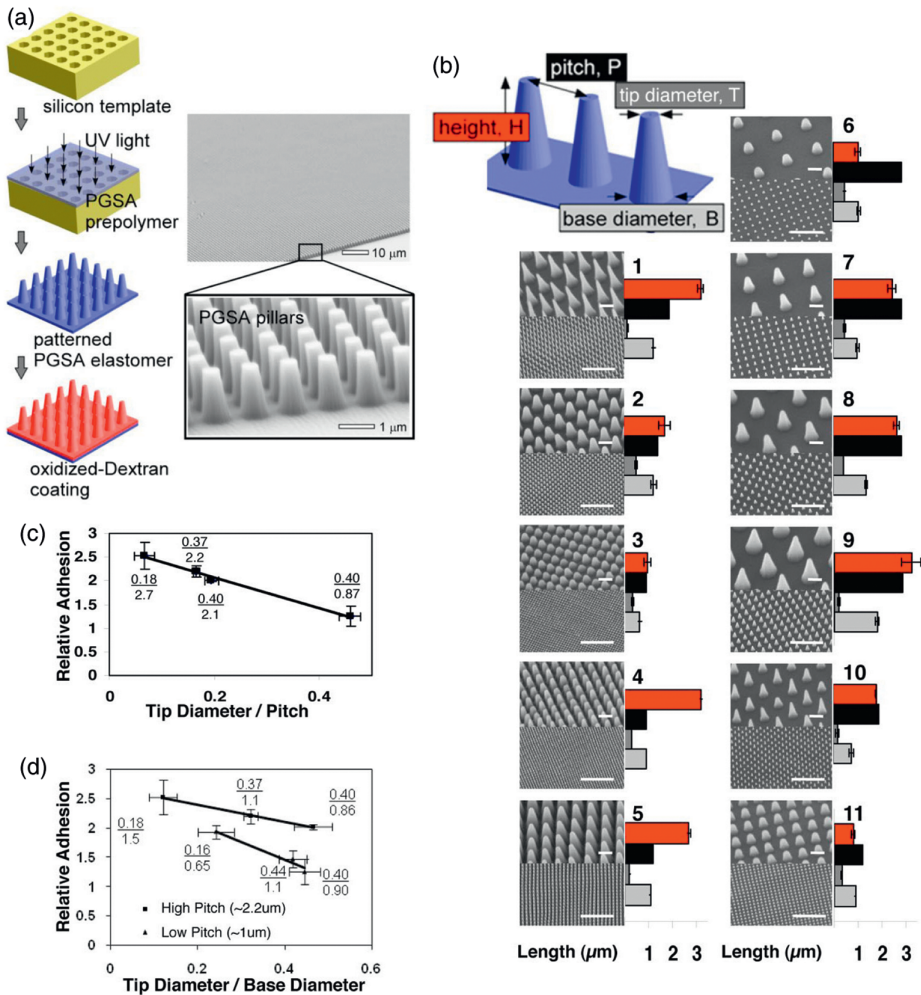


Figure 1.18 Development of biodegradable synthetic gecko patterns. (a) Nanomolding of the GSA prepolymer is accomplished by photocuring the prepolymer under UV light, followed by removal of the pattern and subsequent spin coating of DXTA on the surface of the pillars. SEM imaging demonstrated excellent pattern transfer and fidelity; (b) Gecko patterns having different pillar size and center-to-center pitch were developed, as illustrated in the SEM images. Pillar dimensions were measured by using optical profilometry, as represented by the bar graphs, with red representing the height of pillars; black the center-to-center pitch; light

gray the diameter of pillar base; and dark gray the diameter of the tip. Small and large scale bars are 1 and 10 μm, respectively; (c) Adhesion trend of the longest pillar heights (2.4 μm) shows adhesion of the nanopattern with respect to flat polymer as a function of ratio of tip diameter to pitch. The R^2 value of linear fit was 0.99; (d) Adhesion trend of the patterns plotted as a function of the ratio of tip diameter to base diameter of pillars. The R^2 values of linear fits for the low- and high-pitch patterns were 0.96 and 0.99, respectively. Reprinted from Ref. [111]; © 2008, National Academy of Sciences, USA.

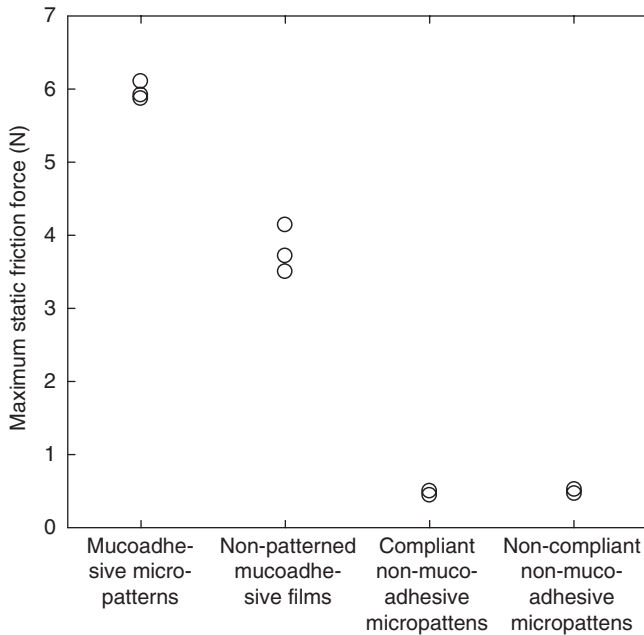


Figure 1.19 Maximum static friction after shearing along the colonic surface of the different samples prepared by Dodou *et al.* The data show the superior behavior of the structured mucoadhesive patterns. Reprinted with permission from Ref. [112].

biodegradable; taken together, these properties demonstrated the great promise for these adhesives as medical materials. In a subsequent feature article, Yanik [12] predicted that the cost of such adhesives might fall to US\$ 10 for a 5–8 cm patch, making them attractive for future applications as sutures and bandages.

One other area of medicine where fibrillar structures might have future use is that of *drug delivery systems*. Fischer *et al.* [11] proposed that silicon nanowire-coated microspheres would adhere better to a mucous layer than would spheres coated with targeting agents, and tested these superior adhesive properties in both shear and lift-off experiments. As adhesion to mucous layers is important not only for drug delivery systems but also for endoscopic devices, gecko-inspired structures might lead to the creation of new designs that would be much more comfortable and less traumatic for the patient. Dodou *et al.* [112] patterned a mucoadhesive film with micron-sized pillars and compared its performance to a nonstructured film (Figure 1.19). Subsequent *in vitro* experiments showed that the friction of the structured film was significantly higher than that of the flat film, and that the grip generated by the micropatterns far exceeded that of the flat mucoadhesive film. The main benefit of these adhesives is that they would interact only with the mucous layer, without affecting the colonic epithelium (as is the case with current endoscopes). A similar concept was proposed by Glass *et al.* [113], who created a

three-legged anchoring mechanism capable of enhancing existing passive-capsule endoscopes. In this case, the dry PDMS-based micropillars showed a 50–100% improvement over an unstructured material in terms of friction, which was tested *in vitro* using fresh porcine small intestine samples. However, when the pillars were coated with a thin layer of silicon oil, the frictional properties were increased by up to 400% over the flat samples. The structures were also tested in a simulated intestine environment, demonstrating their potential for use in the human body. Interestingly, these authors built a prototype working robot that weighed only 10 g, and was capable of maneuvering in the simulated intestine material.

The examples described here demonstrate the great potential of bioinspired fibrillar adhesives in the life sciences. It is clear that future research will not only refine current applications, but also open many new doors not yet considered.

1.7

Summary and Future Perspectives

In recent years, studies of biological systems have shown clearly that the strategy of contact splitting leads to a novel control of adhesion, providing both enhanced strength and manageable release. Inspired by these beautiful examples, several research groups have employed well-established and recently developed methods for patterning materials surfaces to create synthetic analogs of Nature. Based on the mechanisms for pattern control of adhesion, the following conclusions can be drawn:

- **Contact splitting:** Reducing the size of the contacting fibers will increase the adhesion performance. The gain in pull-off force—the splitting efficiency—depends heavily on the contact shape.
- **Shape effect:** The shape of the terminal element has a very strong effect on the adhesion of the fibrillar interface. Each shape has a different splitting efficiency; the shape with the highest efficiency and the strongest overall adhesion is the mushroom-shaped pillar.
- **Fiber aspect ratio:** The higher the fiber aspect ratio, the greater the pull-off force. An increase in compliance is also important when making contact with rough surfaces.
- **Young's modulus:** The softer the fiber, the higher the pull-off force.
- **Backing layer thickness:** A thinner backing layer leads to a stronger adhesive.
- **Hierarchy:** Depending on the packing density and the tip geometry, different behaviors have been identified. For mushroom-shaped pillars, a significant increase in adhesion was reported.
- **Parameter space:** The parameter space for designing fibrillar adhesives is vast. One interesting approach to visualize the most important design variables involved the creation of *adhesion design maps*. These were recently expanded to

take into account different tip shapes and surface roughness. Whilst the latter parameter will be crucial in real life applications, it has not yet been addressed, but will surely become one of the major challenges ahead.

- **Future developments:** Many fascinating questions await answers, one being to mimic the self-cleaning capability of the gecko system. Another area where much research effort has been made [114, 115] is in the field of frictional adhesion, or the frictional behavior of fibrillar systems. Whilst details of this are beyond the scope of this chapter, interesting observations have been made showing that the frictional behavior of a fibrillar interface is superior to that of its unstructured counterpart.
- **Life science applications:** As noted above, the first steps in developing gecko-inspired adhesives for applications in the life sciences have been taken. A biocompatible and biodegradable fibrillar adhesive with very good adhesion properties has been developed, and its potential use for sealing wounds and for suture and staple replacement has been demonstrated. A fibrillar structure has also been investigated for drug delivery systems. Another very promising field, where many patients might benefit from bioinspired adhesives, is that of gastroendoscopy. Here, mucoadhesive interfaces with sufficient adhesion have enabled the development of new endoscopes that are far less traumatic for the patient, and significantly reduce the risk of severe complications during endoscopy. This is possible because the adhesives interact only with the mucous layer, and not with the colonic epithelium. Moreover, such endoscopes can be made much smaller than their current counterparts, allowing them to make sharp turns inside the colon so as to reduce the risk of colonic structural damage. Whilst future developments will optimize fibrillar interfaces for current applications, new fields of application will surely be identified.

References

- 1 Aristotle (350 B.C.) (1918) *Historia Animalium, Historia Animalium*, (translated by D.A.W. Thomson), Clarendon, Oxford.
- 2 Hiller, U. (1968) Untersuchungen zum Feinbau und zur Funktion der Haftborsten in Reptilien. *Zeitschrift Für Morphologie Der Tiere*, **62**, 307–62.
- 3 Hiller, U. and Blaschke, R. (1967) Zum Haftproblem der Gecko-Füsse. *Naturwissenschaften*, **54**, 344–5.
- 4 Autumn, K., Liang, Y.A., Hsieh, S.T., Zesch, W., Chan, W.P., Kenny, T.W., Fearing, R. and Full, R.J. (2000) Adhesive force of a single gecko foot-hair. *Nature*, **405**, 681–5.
- 5 Huber, G., Gorb, S.N., Spolenak, R. and Arzt, E. (2005) Resolving the nanoscale adhesion of individual gecko spatulae by atomic force microscopy. *Biology Letters*, **1**, 2–4.
- 6 Huber, G., Mantz, H., Spolenak, R., Mecke, K., Jacobs, K., Gorb, S.N. and Arzt, E. (2005) Evidence for capillary contributions to gecko adhesion from single spatula nanomechanical measurements. *Proceedings of the National Academy of Sciences of the United States of America*, **102**, 16293–6.
- 7 Arzt, E., Gorb, S. and Spolenak, R. (2003) From micro to nano contacts in biological attachment devices.

- Proceedings of the National Academy of Sciences of the United States of America*, **100**, 10603–6.
- 8 Hansen, W.R. and Autumn, K. (2005) Evidence for self-cleaning in gecko setae. *Proceedings of the National Academy of Sciences of the United States of America*, **102**, 385–9.
 - 9 Chan, E.P., Greiner, C., Arzt, E. and Crosby, A.J. (2007) Designing model systems for enhanced adhesion. *MRS Bulletin*, **32**, 496–503.
 - 10 Del Campo, A. and Arzt, E. (2007) Design parameters and current fabrication approaches for developing bioinspired dry adhesives. *Macromolecular Bioscience*, **7**, 118–27.
 - 11 Fischer, K.E., Aleman, B.J., Tao, S.L., Daniels, R.H., Li, E.M., Bunger, M.D., Nagaraj, G., Singh, P., Zettl, A. and Desai, T.A. (2009) Biomimetic nanowire coatings for next generation adhesive drug delivery systems. *Nano Letters*, **9**, 716–20.
 - 12 Yanik, M.F. (2009) Towards gecko-feet-inspired bandages. *Trends in Biotechnology*, **27**, 1–2.
 - 13 Arzt, E., Enders, S. and Gorb, S. (2002) Towards a micromechanical understanding of biological surface devices. *Zeitschrift für Metallkunde*, **93**, 345–51.
 - 14 Kaelble, D.H. (1960) Theory and analysis of peel adhesion—bond stresses and distributions. *Transactions of the Society of Rheology*, **4**, 45–73.
 - 15 Crosby, A.J., Hageman, M. and Duncan, A. (2005) Controlling polymer adhesion with “pancakes”. *Langmuir*, **21**, 11738–43.
 - 16 Greiner, C., del Campo, A. and Arzt, E. (2007) Adhesion of bioinspired micropatterned surfaces: effects of pillar radius, aspect ratio and preload. *Langmuir*, **23**, 3495–502.
 - 17 Del Campo, A., Greiner, C. and Arzt, E. (2007) Contact shape controls adhesion of bioinspired fibrillar surfaces. *Langmuir*, **23**, 10235–43.
 - 18 Thomas, T. and Crosby, A.J. (2006) Controlling adhesion with surface hole patterns. *Journal of Adhesion*, **82**, 311–29.
 - 19 Varenberg, M., Peressadko, A., Gorb, S. and Arzt, E. (2006) Effect of real contact geometry on adhesion. *Applied Physics Letters*, **89**, 121905.
 - 20 Chan, E.P., Ahn, C.H. and Crosby, A.J. (2007) Adhesion of patterned reactive interfaces. *Journal of Adhesion*, **83**, 473–89.
 - 21 Maugis, D. and Barquins, M. (1978) Fracture mechanics and the adherence of viscoelastic bodies. *Journal of Physics D: Applied Physics (UK)*, **11**, 1989–2023.
 - 22 Johnson, K.L., Kendall, K. and Roberts, A.D. (1971) Surface energy and contact of elastic solids. *Proceedings of the Royal Society of London Series A*, **324**, 301–13.
 - 23 Gao, H.J. and Yao, H.M. (2004) Shape insensitive optimal adhesion of nanoscale fibrillar structures. *Proceedings of the National Academy of Sciences of the United States of America*, **101**, 7851–6.
 - 24 Spolenak, R., Gorb, S. and Arzt, E. (2005) Adhesion design maps for bio-inspired attachment systems. *Acta Biomaterialia*, **1**, 5–13.
 - 25 Greiner, C., Buhl, S., Del Campo, A. and Arzt, E. (2009) Experimental parameters controlling adhesion of biomimetic fibrillar surfaces. *Journal of Adhesion*, **85**, 646–61.
 - 26 Greiner, C., Spolenak, R. and Arzt, E. (2009) Adhesion design maps for fibrillar adhesives: the effect of shape. *Acta Biomaterialia*, **5**, 597–606.
 - 27 Whitesides, G.M., Ostuni, E., Takayama, S., Jiang, X.Y. and Ingber, D.E. (2001) Soft lithography in biology and biochemistry. *Annual Review of Biomedical Engineering*, **3**, 335–73.
 - 28 Xia, Y.N. and Whitesides, G.M. (1998) Soft lithography. *Angewandte Chemie, International Edition in English*, **37**, 551–75.
 - 29 Glassmaker, N.J., Jagota, A., Hui, C.Y. and Kim, J. (2004) Design of biomimetic fibrillar interfaces: 1. making contact. *Journal of the Royal Society, Interface*, **1**, 23–33.
 - 30 Lamblet, M., Verneuil, E., Vilmin, T., Buguin, A., Solberzan, P. and Léger, L. (2007) Adhesion enhancement through micropatterning at polydimethylsiloxane-acrylic adhesive interfaces. *Langmuir*, **23**, 6966–74.
 - 31 Sitti, M. and Fearing, R.S. (2003) Synthetic gecko foot-hair micro/

- nano-structures as dry adhesives. *Journal of Adhesion Science and Technology*, **17**, 1055–73.
- 32 Peressadko, A. and Gorb, S.N. (2004) When less is more: experimental evidence for tenacity enhancement by division of contact area. *Journal of Adhesion*, **80**, 247–61.
 - 33 del Campo, A. and Greiner, A. (2007) SU-8: a photoresist for high-aspect-ratio and 3D submicron lithography. *Journal of Micromechanics and Microengineering*, **17**, R81–95.
 - 34 Aksak, B., Murphy, M.P. and Sitti, M. (2007) Adhesion of biologically inspired vertical and angled polymer microfiber arrays. *Langmuir*, **23**, 3322–32.
 - 35 Federle, W. (2006) Why are so many adhesive pads hairy? *Journal of Experimental Biology*, **209**, 2611–21.
 - 36 Murphy, M.P., Aksak, B. and Sitti, M. (2009) Gecko-inspired directional and controllable adhesion. *Small*, **5**, 170–5.
 - 37 Pokroy, B., Epstein, A.K., Persson-Gulda, M.C.M. and Aizenberg, J. (2009) Fabrication of bioinspired actuated nanostructures with arbitrary geometry and stiffness. *Advanced Materials*, **21**, 463–9.
 - 38 Jeong, H.E., Lee, S.H., Kim, J.K. and Suh, K.Y. (2006) Nanoengineered multiscale hierarchical structures with tailored wetting properties. *Langmuir*, **22**, 1640–5.
 - 39 Yoon, E.S., Singh, R.A., Kong, H., Kim, B., Kim, D.H., Jeong, H.E. and Suh, K.Y. (2006) Tribological properties of bio-mimetic nano-patterned polymeric surfaces on silicon wafer. *Tribology Letters (USA)*, **21**, 31–7.
 - 40 Majidi, C., Groff, R.E. and Fearing, R. (2003) Clumping and packing of hair arrays manufactured by nanocasting. Presented at *IEEE-NANO, San Francisco*.
 - 41 Jin, M., Feng, X., Feng, L., Sun, T., Zhai, J., Li, T. and Jiang, L. (2005) Superhydrophobic aligned polystyrene nanotube films with high adhesive force. *Advanced Materials*, **17**, 1977–81.
 - 42 Kim, D.S., Lee, H.S., Lee, J., Kim, S., Lee, K.H., Moon, W. and Kwon, T.H. (2007) Replication of high-aspect-ratio nanopillar array for biomimetic gecko foot-hair prototype by UV nano embossing with anodic aluminium oxide mold. *Microsystem Technologies*, **13**, 601–6.
 - 43 Kim, S., Kustandi, T.S. and Yi, D.-K. (2008) Synthesis of artificial polymeric nanopillars for clean and reusable adhesives. *Journal of Nanoscience and Nanotechnology*, **8**, 4779–82.
 - 44 Geim, A.K., Dubonos, S.V., Grigorieva, I.V., Novoselov, K.S., Zhukov, A.A. and Shapoval, S.Y. (2003) Microfabricated adhesive mimicking gecko foot-hair. *Nature Materials*, **2**, 461–3.
 - 45 Qu, L. and Dai, L. (2007) Gecko-Foot-Mimetic aligned single-walled carbon nanotube dry adhesives with unique electrical and thermal properties. *Advanced Materials*, **19**, 3844–9.
 - 46 Yurdumakan, B., Ravavikar, N.R., Ajayan, P.M. and Dhinojwala, A. (2005) Synthetic gecko foot-hairs from multiwalled carbon nanotubes. *Chemical Communications*, 3799–801.
 - 47 Ge, L., Sethi, S., Ci, L., Ajayan, P.M. and Dhinojwala, A. (2007) Carbon nanotube-based synthetic gecko tapes. *Proceedings of the National Academy of Sciences of the United States of America*, **104**, 10792–5.
 - 48 Zhao, Y., Tong, T., Delzeit, L., Kashani, A., Meyyappan, M. and Majumdar, A. (2006) Interfacial energy and strength of multiwalled-carbon-nanotube-based dry adhesive. *Journal of Vacuum Science and Technology B*, **24**, 331–5.
 - 49 Maeno, Y. and Nakayama, Y. (2009) Geckolike high shear strength by carbon nanotube fiber adhesives. *Applied Physics Letters*, **94**, 012103.
 - 50 Lu, H., Goldman, J., Ding, F., Sun, Y., Pulikkathara, M.X., Khabashesku, V.N., Jakobson, B.I. and Lou, J. (2008) *Friction and Adhesion Properties of Vertically Aligned Multi-Walled Carbon Nanotube Arrays and Fluoro-Nanodiamond Films*, Carbon, online publication.
 - 51 La Spina, G., Stefanini, C., Menciassi, A. and Dario, P. (2005) A novel technological process for fabricating micro-tips for biomimetic adhesion. *Journal of Micromechanics and Microengineering*, **15**, 1576–87.
 - 52 Harfenist, S.A., Cambron, S.D., Nelson, E.W., Berry, S.M., Isham, A.W., Crain, M.M., Walsh, K.M., Keynton, R.S. and Cohn, R.W. (2004) Direct drawing of

- suspended filamentary micro- and nanostructures from liquid polymers. *Nano Letters*, **4**, 1931–7.
- 53 Jeong, H.E., Lee, S.H., Kim, P. and Suh, K.Y. (2006) Stretched polymer nanohairs by nanodrawing. *Nano Letters*, **6**, 1508–13.
- 54 Greiner, C., Arzt, E. and Del Campo, A. (2008) Hierarchical gecko-like adhesives. *Advanced Materials*, **21**, 479–82.
- 55 Northen, M.T. and Turner, K.L. (2005) A batch fabricated biomimetic dry adhesive. *Nanotechnology*, **16**, 1159–66.
- 56 Northen, M.T. and Turner, K.L. (2006) Meso-scale adhesion testing of integrated micro- and nano-scale structures. *Sensors and Actuators. A, Physical*, **130–131**, 583–7.
- 57 Northen, M.T., Greiner, C., Arzt, E. and Turner, K.L. (2008) A gecko-inspired reversible adhesive. *Advanced Materials*, **20**, 3905–9.
- 58 Murphy, M.P., Kim, S. and Sitti, M. (2009) Enhanced adhesion by gecko-inspired hierarchical fibrillar adhesives. *ACS Applied Materials and Interfaces*, **1**, 849–55.
- 59 Kustandi, T.S., Samper, V.D., Ng, W.S., Chong, A.S. and Gao, H. (2007) Fabrication of a gecko-like hierarchical fibril array using a bonded porous alumina template. *Journal of Micromechanics and Microengineering*, **17**, N75–81.
- 60 Spolenak, R., Gorb, S., Gao, H.J. and Arzt, E. (2005) Effects of contact shape on the scaling of biological attachments. *Proceedings of the Royal Society of London Series A—Mathematical Physical and Engineering Sciences*, **461**, 305–19.
- 61 Del Campo, A., Greiner, C., Álvarez, I. and Arzt, E. (2007) Patterned surfaces with pillars with controlled and 3D tip geometry mimicking bioattachment devices. *Advanced Materials*, **19**, 1973–7.
- 62 del Campo, A., Álvarez, I., Filipe, S. and Wilhelm, M. (2007) 3D microstructured surfaces obtained by soft-lithography using fast-crosslinking elastomeric precursors and 2D masters. *Advanced Functional Materials*, **17**, 3590–7.
- 63 Glassmaker, N.J., Jagota, A., Hui, C.Y., Noderer, W.L. and Chaudhury, M.K. (2007) Biologically inspired crack trapping for enhanced adhesion. *Proceedings of the National Academy of Sciences of the United States of America*, **104**, 10786–91.
- 64 Kim, S. and Sitti, M. (2006) Biologically inspired polymer microfibers with spatulate tips as repeatable fibrillar adhesives. *Applied Physics Letters*, **89**, 261911.
- 65 Reddy, S., Del Campo, A. and Arzt, E. (2007) Bioinspired surfaces with switchable adhesion. *Advanced Materials*, **19**, 3833–7.
- 66 Reddy, S., Arzt, E. and Del Campo, A. (2007) Bioinspired surfaces with switchable adhesion. *Advanced Materials*, **19**, 3833–7.
- 67 Lin, P.-C., Vajpayee, S., Jagota, A., Hui, C.Y. and Yang, S. (2008) Mechanically tunable dry adhesive from wrinkled elastomers. *Soft Matter*, **4**, 1830–5.
- 68 Xie, T. and Xiao, X.C. (2008) Self-peeling reversible dry adhesive system. *Chemistry of Materials*, **20**, 2866–8.
- 69 Shull, K.R., Ahn, D., Chen, W.L., Flanigan, C.M. and Crosby, A.J. (1998) Axisymmetric adhesion tests of soft materials. *Macromolecular Chemistry and Physics*, **199**, 489–511.
- 70 Shull, K.R. (2002) Contact mechanics and the adhesion of soft solids. *Materials Science and Engineering Reports*, **36**, 1–45.
- 71 Greiner, C., Buhl, S., Del Campo, A. and Arzt, E. (2009) Experimental parameters controlling adhesion of biomimetic fibrillar surfaces. *Journal of Adhesion*, **85**, 646–61.
- 72 Kustandi, T.S., Samper, V.D., Yi, D.-K., Ng, W.-S., Neuzil, P. and Sun, W. (2007) Self-assembled nanoparticles based fabrication of gecko foot-hairs inspired polymer nanofibers. *Advanced Functional Materials*, **17**, 2211–18.
- 73 Varenberg, M., Peressadko, A., Gorb, S., Arzt, E. and Mrotzek, S. (2006) Advanced testing of adhesion and friction with a microtribometer. *Review of Scientific Instruments*, **77**, 066105.
- 74 Murphy, M.P., Aksak, B. and Sitti, M. (2007) Adhesion and anisotropic friction enhancements of angled heterogeneous micro-fiber arrays with spherical and

- spatula tips. *Journal of Adhesion Science and Technology*, **21**, 1281–96.
- 75 Cheung, E. and Sitti, M. (2008) Adhesion biological inspired oil-coated polymer micropillars. *Journal of Adhesion Science and Technology*, **22**, 569–89.
- 76 Peressadko, A., Hosoda, N. and Persson, B.N.J. (2005) Influence of surface roughness on adhesion between elastic bodies. *Physical Review Letters*, **95**, 124301.
- 77 Glassmaker, N.J., Jagota, A. and Hui, C.Y. (2005) Adhesion enhancement in a biomimetic fibrillar interface. *Acta Biomaterialia*, **1**, 367–75.
- 78 Hui, C.Y., Glassmaker, N.J., Tang, T. and Jagota, A. (2004) Design of biomimetic fibrillar interfaces: 2. mechanics of enhanced adhesion. *Journal of the Royal Society, Interface*, **1**, 35–48.
- 79 Liu, J., Hui, C.Y., Shen, L. and Jagota, A. (2008) Compliance of a microfibril subjected to shear and normal loads. *Journal of the Royal Society, Interface*, **5**, 1087–97.
- 80 Kim, S., Sitti, M., Hui, C.Y., Long, R. and Jagota, A. (2007) Effect of backing layer thickness on adhesion of single-level elastomer fiber arrays. *Applied Physics Letters*, **91**, 161905.
- 81 Yao, H., Della Rocca, G., Guduru, P.R. and Gao, H. (2007) Adhesion and sliding response of a biologically inspired fibrillar surface: experimental observations. *Journal of the Royal Society, Interface*, **5**, 723–33.
- 82 Verneuil, E., Ladoux, B., Buguin, A. and Silberzan, P. (2007) Adhesion on microstructured surfaces. *Journal of Adhesion*, **83**, 449–72.
- 83 Santos, D., Spenko, M., Parness, A., Kim, S. and Cutkosky, M. (2007) Directional adhesion for climbing: theoretical and practical considerations. *Journal of Adhesion Science and Technology*, **21**, 1317–41.
- 84 Northen, M.T. and Turner, K.L. (2006) Batch fabrication and characterization of nanostructures for enhanced adhesion. *Current Applied Physics*, **6**, 379–83.
- 85 Pfaff, H. (2005) Synthesis and adhesion of biomimetic contact elements, Ph.D. Thesis, Fakultät Chemie, Universität Stuttgart.
- 86 Huber, G., Gorb, S.N., Hosoda, N., Spolenak, R. and Arzt, E. (2007) Influence of surface roughness on gecko adhesion. *Acta Biomaterialia*, **3**, 607–10.
- 87 Jagota, A. and Bennisson, S.J. (2002) Mechanics of adhesion through a fibrillar microstructure. *Integrative and Comparative Biology*, **42**, 1140–5.
- 88 Lake, G.J. and Thomas, A.G. (1967) Strength of highly elastic materials. *Proceedings of the Royal Society of London Series A – Mathematical and Physical Sciences*, **300**, 108–19.
- 89 Gorb, S., Varenberg, M., Peressadko, A. and Tuma, J. (2006) Biomimetic mushroom-shaped fibrillar adhesive microstructure. *Journal of the Royal Society, Interface*, **4**, 271–5.
- 90 Kim, S., Aksak, B. and Sitti, M. (2007) Enhanced friction of elastomer microfiber adhesives with spatulate tips. *Applied Physics Letters*, **91**, 221913.
- 91 Kim, S., Cheung, E. and Sitti, M. (2009) Wet Self-Cleaning of biologically inspired elastomer mushroom shaped microfibrillar adhesives. *Langmuir*, **25**, 7196–9.
- 92 Hertz, H. (1882) Über die Berührung fester elastischer Körper. *Journal für die Reine und Angewandte Mathematik*, **92**, 156–71.
- 93 Shen, L., Glassmaker, N.J., Jagota, A. and Hui, C.Y. (2008) Strongly enhanced static friction using a film-terminated fibrillar interface. *Soft Matter*, **4**, 618–25.
- 94 Noderer, W.L., Shen, L., Vajpayee, S., Glassmaker, N.J., Jagota, A. and Hui, C.Y. (2007) Enhanced adhesion and compliance of film-terminated fibrillar surfaces. *Proceedings of the Royal Society of London Series A - Mathematical Physical and Engineering Sciences*, **463**, 2631–54.
- 95 Yao, H. and Gao, H. (2007) Mechanical principles of robust and releasable adhesion of gecko. *Journal of Adhesion Science and Technology*, **21**, 1185–212.
- 96 Yao, H. and Gao, H. (2007) Bio-inspired mechanics of bottom-up designed hierarchical materials: robust and releasable adhesion systems of gecko. *Bulletin of the Polish Academy of Sciences - Technic and Science*, **55**, 141–50.

- 97 Yao, H. and Gao, H. (2006) Mechanics of robust and releasable adhesion in biology: bottom-up designed hierarchical structures of gecko. *Journal of the Mechanics and Physics of Solids*, **54**, 1120–46.
- 98 Bhushan, B., Peressadko, A. and Kim, T.W. (2006) Adhesion analysis of two-level hierarchical morphology in natural attachment systems for “smart adhesion”. *Journal of Adhesion Science and Technology*, **20**, 1475–91.
- 99 Kim, T.W. and Bhushan, B. (2007) Effect of stiffness of multi-level hierarchical attachment systems on adhesion enhancement. *Ultramicroscopy*, **107**, 902–12.
- 100 Porwal, P.K. and Hui, C.Y. (2008) Strength statistics of adhesive contact between a fibrillar structure and a rough substrate. *Journal of the Royal Society, Interface*, **5**, 441–8.
- 101 Varenberg, M. and Gorb, S. (2007) Shearing of fibrillar adhesive microstructure: friction and shear-related changes in pull-off force. *Journal of the Royal Society, Interface*, **4**, 721–5.
- 102 Ghatak, A., Mahadevan, L., Chung, J.Y., Chaudhury, M.K. and Shenoy, V. (2004) Peeling from a biomimetically patterned thin elastic film. *Proceedings of the Royal Society of London A—Mathematical Physical and Engineering Sciences*, **460**, 2725–35.
- 103 Majumder, A., Ghatak, A. and Sharma, A. (2007) Microfluidic adhesion induced by subsurface microstructures. *Science*, **318**, 258–61.
- 104 Sethi, S., Ge, L., Ci, L., Ajayan, P.M. and Dhinojwala, A. (2008) Gecko-inspired carbon nanotube-based self-cleaning adhesives. *Nano Letters*, **8**, 822–5.
- 105 Lee, J. and Fearing, R. (2008) Contact self-cleaning of synthetic gecko adhesive from polymer microfibers. *Langmuir*, **24**, 10587–91.
- 106 Schubert, B., Lee, J., Majidi, C. and Fearing, R. (2008) Sliding-induced adhesion of stiff polymer microfiber arrays. II. Microscale behavior. *Journal of the Royal Society, Interface*, **5**, 845–53.
- 107 Lee, J., Majidi, C., Schubert, B. and Fearing, R. (2008) Sliding-induced adhesion of stiff polymer microfiber array. I. Macroscale behavior. *Journal of the Royal Society, Interface*, **5**, 835–44.
- 108 Buhl, S., Greiner, C., Del Campo, A. and Arzt, E. (2009) Humidity effect on adhesion of microstructured elastomer surfaces. *International Journal of Materials Research*, **100**, 1119–26.
- 109 Lee, H., Lee, B.P. and Messersmith, P.B. (2007) A reversible wet/dry adhesive inspired by mussels and geckos. *Nature*, **448**, 338–42.
- 110 Varenberg, M. and Gorb, S. (2008) A beetle-inspired solution for underwater adhesion. *Journal of the Royal Society, Interface*, **5**, 383–5.
- 111 Mahdavi, A., Ferreira, L., Sundback, C., Nichol, J.W., Chan, E.P., Carter, D.J.D., Bettinger, C.J., Patanavanich, S., Chignozha, L., Ben-Joseph, E., Galakatos, A., Pryor, H., Pomerantseva, I., Masiakos, P.T., Faquin, W., Zumbuehl, A., Hong, S., Borenstein, J., Vacanti, J., Langer, R. and Karp, J.M. (2008) A biodegradable and biocompatible gecko-inspired tissue adhesive. *Proceedings of the National Academy of Sciences of the United States of America*, **105**, 2307–12.
- 112 Dodou, D., del Campo, A. and Arzt, E. (2007) Mucoadhesive micropatterns for enhanced grip. Conference Proceedings of the IEEE Engineering Medicine Biology Society, 2007.
- 113 Glass, P., Cheung, E. and Sitti, M. (2008) A legged anchoring mechanism for capsule endoscopes using micropatterned adhesives. *IEEE Transactions on Bio-Medical Engineering*, **55**, 2759–67.
- 114 Shen, L., Jagota, A. and Hui, C.Y. (2009) Mechanism of sliding friction on a film-terminated fibrillar interface. *Langmuir*, **25**, 2772–80.
- 115 Vajpayee, S., Long, R., Shen, L.L., Jagota, A. and Hui, C.Y. (2009) Effect of rate on adhesion and static friction of a film-terminated fibrillar interface. *Langmuir*, **25**, 2765–71.

